Acta Geochim (2020) 39(3):365–386
https://doi.org/10.1007/s11631-019-00363-9

ORIGINAL ARTICLE

Trace elemental signatures and mineral chemistry of clays associated with the alteration halos of the Paleoproterozoic U mineralization in Bijawars of the Sonrai Basin, Central India

Surendra Kumar Jha[1,2] · Rashmi Sharma[1] · Jaya Prakash Shrivastava[1]

Received: 2 November 2018 / Revised: 19 June 2019 / Accepted: 12 July 2019 / Published online: 18 July 2019

Abstract Paleoproterozoic Bijawars of the Sonrai basin consists of (a) Sonrai (mostly carbonate carbonaceous shale and phosphatic breccia) and (b) Solda Formations (commonly chloritic and ferruginous shale) with well-developed clay-organo-rich facies, often marked with hydrothermal activities. Previous studies revealed abundance order of kaolinite > chlorite > illite > smectite; and kaolinite > illite > chlorite in clay (0.2–2.0 μm) fractions separated from the Sonrai and Solda Formations, respectively. To understand atomic substitutions and trace elemental concentrations, clay minerals were analyzed by fusion ICP-MS and SEM–EDS. PAAS normalized data plots show U, Th, Rb, Ba, Pb Sr, and large-ion lithophiles enrichment, whereas, Bandai sandstone and Rohini carbonate clays show HREE enrichment with asymmetrical patterns, similar to those reported from the well-established McArthur River, Cigar Lake, and Sue UTUD of Canada. For Rohni carbonate, chondrite-normalized REE data plots revealed M shape REE patterns, ascribed to Gd–Tb–Dy–Ho tetrad effect and anomalous Y, Zr, and Hf concentrations. Owing to HREE incorporation in the clay inter-layers, linear and flattened REE trends were noticed. Flat REE patterns associated with the highly altered chlorite and illite represent negative Eu anomaly related to the dilational nature of the uraninite structure and is suggestive of anoxic conditions.

Keywords Bijawars · Sonrai basin · Clays · REE patterns · Uranium mineralization

1 Introduction

The Paleoproterozoic, intra-cratonic, and siliciclastic Bijawar Group (2–1.4 Ga) of rocks in the marginal Sonrai basin (Fig. 1) overlies the Archean Bundelkhand Basement Complex (3.3–2.5 Ga) and lies below theVindhyan Supergroup (1.4–0.5 Ga) with unconformable contacts (cited Table 1: Jha et al. 2012). The Sonrai basin is rectilinear in shape, trending in the E–W directions and dipping gently in southern direction, covers an area of 28 km in length and 5–7 km in width. In the Sonrai basin, the Bijawar sequence rests unconformably over the pre-existing Berwar Formation (Sharma and Rahman 2000), where mafic-ultramafics of the Madaura Formation cut across the Berwar Formation and Basement Gneissic Complex (Prakash et al. 1975). In this area, E–W faults represent reactivation of rift-related earlier faults in the granitic basement (Prakash et al. 1975; Srivastava 1989). The stratigraphy of the area (cited Table 1: Jha et al. 2012) proposed by Prakash et al. (1975) sub-divided Bijawar rocks into (a) Sonrai and (b) Solda Formations. The former is further sub-divided into Jamuni carbonate, Gorakalan shale, Rohini quartzite, Rohini carbonate, and Bandai sandstone (including Kurrat volcanic), whereas, the latter is sub-divided into Chloritic shale, Dhorisagar, and Solda quartzite as members (Fig. 1). The Sonrai Formation unconformably overlies the Mehroni Group and is marked by a basal conglomerate. U mineralization occurs at or near the

Electronic supplementary material The online version of this article (https://doi.org/10.1007/s11631-019-00363-9) contains supplementary material, which is available to authorized users.

✉ Jaya Prakash Shrivastava
jpshrivastava.du@gmail.com

[1] University of Delhi, Delhi, India

[2] Present Address: Department of Cement Technology, A.K.S. University, Satna, MP, India

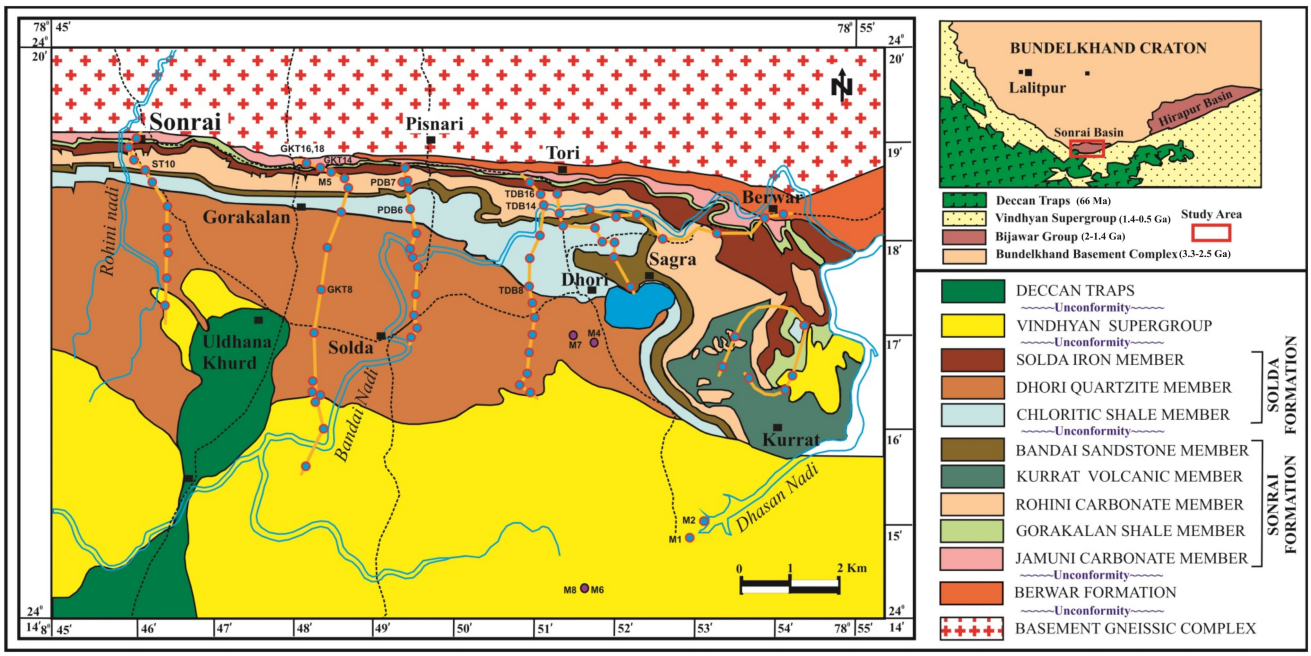

Fig. 1 Geological map (modified after, Prakash et al. 1975) of the Palaeoproterozoic Sonrai basin, Central India

unconformable contacts between regionally metamorphosed Archaean to Lower Proterozoic basement and Lower to Middle Proterozoic (1900–1200 Ma) continental clastic sediments. Moreover, Roy et al. (2004) reported the dominance of pitchblende with a minor amount of U silicate in this area. Recently, Rawat et al. (2018) reported uranium-bitumen association within the fractures of the Gorakalan shale, Rohini carbonate, and Bandai sandstone of the Sonrai as well as lower chloritic shale of the Solda Formation. In Paleoproterozoics of the Sonrai basin, mineralization occurs at two different stratigraphic levels in dolomite and pelite-arenite horizons of the Rohini carbonate and Chloritic shale, respectively.

Illite and chlorite are commonly associated with the sedimentary rocks (Daniels and Altaner 1990) and hydrothermal alteration halos. Morichon et al. (2010) discussed that clay minerals occur in the unconformity-type uranium mineralization (UTUM). Clay mineral assemblages form major constituents of an alteration halo around Proterozoic UTUM (Hoeve and Quirt 1987; Percival and Kodama 1989; Iida 1993; Pacquet and Weber 1993). Beaufort et al. (2005) reported a variety of clay mineral assemblages in the Proterozoic UTUM. Thus, chlorite and illite have been used to comprehend the nature, origin, and timing of the fluids that altered Precambrian granites as well as overlying rock in the Sonrai basin. Jha et al. (2012) on the basis of needle shape (trans-vacant) *tv*-1*M* polytype, illite and inter-stratified mixed smectite (Sm)/illite (Ill) or Sm/chlorite (Chl) in the Jamuni and Rohini carbonate and Bandai sandstone, suggested high fluid/rock interaction under hydrothermal conditions.

Sorption and adsorption of the uranyl ions onto clay structures are causative for the removal of U ions from the solution (Borovec 1981). Organic substances interact with the uranyl ions and form soluble complexes which are responsible for ionic precipitation via reduction, adsorption, ion exchange or other sorption processes and modify entrapment in clay structure, thus, affecting depositional mechanism, diagenesis, and hydrothermal processes (Wood 1996). Kister et al. (2006) proposed several chemical and geological conditions conducive to the formation of U deposits. In this area, Prakash et al. (1975) reported uranium-bitumen and Cu–Pb–Zn veins occupying fractures of Bandai and Gorakalan shale, but, Mahadevan (1986) discussed that the U mineralization is hosted within the sandstone inter-bedded with the carbonate rocks. Additionally, Mishra (1996) reported U mineralization in the bituminous shale of the Rohini carbonate. Roy et al. (2014) discussed that the U occurrences are closely associated with the unconformity, separating Sonrai metasediments and the Archean-Paleoproterozoic crystalline basement. Jha et al. (2012) discussed clay-organo-rich facies, structural discontinuities, and frequent hydrothermal alterations together with the fault-bounded nature of the basement as favorable sites for U mineralization in the Sonrai basin. Clay minerals control trace (especially rare earth elements) elemental abundance as they are immobile and adsorbed by the phyllosilicates at the time of weathering (Cullers et al. 1987). Immobile elements undergo

dilution during rock alteration, but extraction causes increase in the trace elemental concentration (Bao et al. 2004). REE content and rocks within the basin have been used to determine paleoenvironmental conditions associated with U deposition (Fayek and Kyser 1997). Moreover, the REE pattern is the most efficient tool for constraining geological models for U deposits (Mercadier et al. 2011). In this area, clay minerals are abundantly present in almost all the major rock types. The clay mineral chemistry is significant in this context. However, clay phyllosilicates and their bearing on uranyl and other associated trace elemental ionic enrichment are yet to be ascertained. Thus, clay structures and associated trace elemental concentrations help to comprehend paleoenvironmental reasons necessary for preferential U enrichment; therefore, present clay compositional studies were carried out with the primary objective to understand clay skeletal structures and possible U in this area.

2 Geological considerations

Generally, UTUM occurs in ancient craton, close to the unconformity between Archaeans and Paleoproterozoic igneous and metamorphic basement with a cover of younger clastic sediments (Pohl 2011). The fertile K-feldspar rich granitic basement bearing a large number of fractures and a high degree of illitization in the Sonrai basin provided an ideal set-up for hosting U mineralization. Similar to other well-established U deposits, Bijawar basin represents a close relationship with the tectonized granitoid basement (with faults and fractures, reactivated fractures) and post-Bijawar faults (Rawat et al. 2010). Moreover, chloritization together with the illitization and kaolinization is also recognized in this area. Thus, present U mineralization complies with these parameters in the Bundelkhand craton and lies close to the unconformity between Archaean and Paleoproterozoic rocks of 3.7–2.24 Ga ages.

3 Materials and methods

For this purpose, 75 fresh samples (each $\sim$ 2 kg.) were collected along 7 traverses, laid down across the E–W trending Sonari basin, covering the Sonrai, Solda, Madaura, and Berwar Formations and spread over the Toposheet No. 54 L/15, (scale of 1:50,000) of the Survey of India (1976) and also over the geological map of the Sonrai basin (Fig. 1). Based on the megascopic characters (Table 1), 19 samples were selected for the analyses.

Prior to trace elemental analysis, 0.2–2.0 μm fraction was separated out from each of the bulk specimens and subjected to washing by disaggregating in distilled water. It was followed by crushing and grinding. Each powdered sample was treated with H_2O_2, CH_3COOH, NaOH (to remove organic matter, carbonates and allophone/silicates, respectively) using a combination of the procedures (Jackson 1969; Wilson 1987; Keil et al. 1994; Yang and Aplin 1997; Tan 2005). The concentration of acid in the residual water was removed by centrifugation. Subsequent to the removal of the suspension, clay fractions were separated out after a specified time interval (based on the settling velocity of the particles), following the dispersion–centrifugation-decantation procedure (Jakson 1985). Samples were finally air dried at 60 °C. For clay mineral identification, oriented mounts prepared by filtering the clay suspension onto a membrane filter and then transferring it onto a glass slide to obtain a uniform diffraction mount and to avoid differential settling of clay particles (Drever 1973). Obtained smears were scanned by an X-ray diffractometer (PANalytical make; X'Pert^3 model) with Cu-Kα radiation at an adopted scanning speed of 1°/min. The internal standard method (Srodon et al. 2001), where, quartz was used as an internal standard, was followed to obtain quantitative results (within an error of < 5 wt%).

Prior to a scanning electron microscopic (SEM) study, clay specimens were transferred onto an adhesive carbon film and characterized by a Carl-Zeiss make; an EVO-MA10 model field emission gun scanning electron microscope (SEM) equipped with an Oxford make (Inca X-Act model) EDXS system at 20 kV voltage and 8 mm working distance after being coated with gold for electrical conductivity. Clay minerals were examined over a range of magnifications as high as 20,000×, but most of the textures were best seen in the range 1000 to 50,000×. To determine major oxides, clay minerals in a window mode, precision better than 1% was maintained throughout EDS analyses and obtained values are presented in Table 1S. To understand chemical composition of clay minerals in terms of atomic ratios in the octahedral, tetrahedral, and interlayers, structural formulae were calculated based on the number of oxygen atoms in the half cell unit and atomic concentration was given on the basis of atom per formula unit (apfu) following the method discussed by Ross and Hendricks (1945) and Weaver (1989). Structural formula calculations imply two basic assumptions (1) anion and cation charges must be equal; the anion charge of half unit cell O_{10} $[OH]_2$ of 2: 1 illite and smectite is equal to 22 and for 2:1: 1 chlorite O_2 $[OH]_8$ it is equal to 28 and (2) the number of tetrahedral cations must be 4.0. Oxide values (in wt%) were converted into atomic proportions. Single cation [SiO_2, MgO, FeO, and CaO (in wt%)] values were divided by their molecular weights, whereas, double cation [$A1_2O_3$ Fe_2O_3, K_2O, and Na_2O] values by the half of their molecular weights. To derive the structural formula, atomic

Table 1 Summarized megascopic characters of rocks of the Sonarai basin

No.	Samples	Fms.	Rocks	Locations (Lat./Long.)	TOC (%)	megascopic Characters
1	M8	Lower Vindhyan	Shale	N 24°14′43.3″ E 78° 51′75.5″	–	Fine gained, thin laminated grey colour shale
2	M6		Shale	N 24°14′43.3″ E 78° 51′75.5″	–	Fine grained, light grey colour laminated, shale
3	M3		Shale	N 24°13′24.4″ E 78° 52′55.9″	–	Dark black, fine grain and laminated, massive shale
4	M2		Vindhyan basal shale	Dhasan river Lakhanjar	–	Reddish brown, fine grained, laminated, ferruginous shale
5	M1		Vindhyan basal shale	Dhasan river Lakhanjar	–	Light grey, fine, laminated shale
6	GKT8	Solda Formation	Dhorisagar shale	N 24°17′37.2″ E 78° 48′20.3″	–	Fine grained, laminated with ferruginous shale.
7	M4		Chloritic shale	N 24°17′11.7″ E 78° 51′51.8″	–	Grey colour, thin laminated, silty shale
8	TDB8		Chloritic shale	N 24°17′01.0″ E 78°51′00.7″	0.11	Dark grey, fine gained, massive, laminated shale
9	PDB6		Chloritic shale	N 24°18′34.1″ E 78°49′29.0″	0.12	Dark grey, fine grained, massive laminated shale
10	M7	Sonrai Formation	Bandai shale	N 24°17′11.7″ E 78° 51′51.8″	–	Dark grey, fine grain shale
11	PDB7		Bandai sandstone	N 24°18′25.0″ E 78°49′31.3″	–	Ferr. dark brown, medium grain, calc-sst.
12	TDB9		Bandai sandstone	N 24°17′14.4″ E 78°51′00.8″	0.09	Fine grained, grey sandstone
13	TDB14		Rohini carbonate	N 24°18′27.8″ E 78°51′06.3″	0.25	Dark grey, siliceous, laminated carbonate
14	TDB16		Rohini carbonate	N 24°18′35.6″ E 78°51′05.5″	0.01	Light grey, laminated, sandy Dolomitic carbonate
15	ST10		Rohini carbonate	N 24°19′05.1″ E 78°45′55.9″	–	Siliceous, arenaceous, grey colour dolomite
16	M5		Gorakalan shale	Gorakalan village	–	Dark black, massive, fine grained shale
17	GKT14		Gorakalan shale	N 24°18′44.0″ E 78°48′19.8″	–	Grey, massive layered, sandy shale
18	GKT18		Graphitic shale	N 24°19′04.0″ E 78°46′23.9″	0.98	Dark, siliceous, fine gained, graphitic shale
19	GKT17		Jamuni carbonate	N 24°19′07.2″ E 78°46′24.1″	–	Pinkish, thin-bedded carbonate with pyrite

– not detected (< 0.01%), *Fms.* formations, *calc*. calcareous, *sst* sandstone, *Ferr*. ferruginous, *Lat*. latitude, *Long*. longitude, *TOC* total organic carbon

proportions multiplied by the K factor obtained by multiplying the atomic proportion of each cation to its valency. Total of these values divided by 22 for 2:1 phyllosilicates and by 28 for 1:1 phyllosilicates.

Major (Table 2) and trace (Table 3) elements were determined by fusion ICP-AES (Inductively Coupled Plasma—Atomic Emission Spectrometry, Model- Thermo Jarrell Ash ENVIRO II) and ICP- MS (Inductively Coupled Plasma Mass Spectrometry, Model: Perkin Elmer Sciex Elan 6000) methods in the Activation Laboratories, Ontario, Canada. For analytical quality control of major and trace elemental data, 20 Geostandards were analyzed intermittently and calculated standard deviation (1σ) values (as detailed in the Electronic Supplement: Tables 2S

Table 2 Major oxides (wt%) and calculated parameters for the Bijawar rocks of the Sonrai basin

Fms.	Sonrai Formation										Solda Formation			
Mems.	Jam. Car	Gor.Shl.			Roh. Car.			Ban. Sst.			Chl. Shl.			Dho. Shl.
Samples	GKT17	GKT18	GKT14	M5	TDB14	TDB16	ST10	TDB9	PDB7	M7	M4	TDB8	PDB6	GKT8
Major oxides														
SiO_2	32.57	67.40	11.37	68.74	40.39	35.46	5.00	89.31	22.92	58.25	47.21	57.12	57.07	25.65
Al_2O_3	5.28	2.97	2.13	12.24	13.99	6.87	1.48	7.81	2.58	20.27	24.68	30.57	13.51	15.59
Fe_2O_3(T)	13.06	2.11	0.55	5.86	5.10	3.22	1.23	1.67	33.37	11.76	10.89	1.58	2.22	6.76
MgO	19.97	1.48	2.04	11.43	17.86	15.24	19.40	0.07	0.71	2.91	3.87	0.33	0.77	0.48
CaO	27.23	0.47	0.39	0.89	16.61	17.33	28.97	0.06	1.45	0.04	0.57	0.09	0.05	0.27
Na_2O	0.03	25.01	83.12	0.14	0.57	19.03	42.37	0.05	35.13	0.04	6.92	6.30	21.64	48.69
K_2O	0.94	0.20	0.17	0.05	3.81	1.93	0.66	0.44	0.55	5.44	5.14	3.69	4.06	2.21
MnO	0.32	0.00	0.00	0.03	0.05	0.06	0.06	0.00	1.79	0.07	0.05	0.00	0.04	0.03
TiO_2	0.28	0.11	0.08	0.52	1.33	0.73	0.08	0.56	0.05	1.17	0.64	0.31	0.59	0.20
P_2O_5	0.32	0.26	0.15	0.10	0.29	0.13	0.77	0.02	1.45	0.03	0.02	0.01	0.05	0.13
Total	100	100	100	100	100	100	100.02	99.99	100	99.98	99.99	100	100	100.01
Calculated parameters														
FeO	6.40	1.03	0.27	2.87	2.50	1.58	0.60	0.82	16.35	5.76	5.34	0.78	1.09	3.31
Fe_2O_3	7.40	1.19	0.31	3.32	2.89	1.83	0.70	0.94	18.91	6.66	6.17	0.90	1.26	3.83
K_2O/Na_2O	na	0.01	0.00	0.33	6.74	0.10	0.02	8.40	0.02	na	0.74	0.59	0.19	0.05
MgO/Al_2O_3	3.78	0.50	0.96	0.93	1.28	2.22	13.13	0.01	0.28	0.14	0.16	0.01	0.06	0.03
K_2O/Al_2O_3	0.18	0.07	0.08	0.00	0.27	0.28	0.45	0.06	0.21	0.27	0.21	0.12	0.30	0.14
Na_2O/Al_2O_3	0.01	8.43	38.94	0.01	0.04	2.77	28.69	0.01	13.64	0.00	0.28	0.21	1.60	3.12
P_2O_5/Al_2O_3	0.06	0.09	0.07	0.01	0.02	0.02	0.52	0.00	0.56	0.00	0.00	0.00	0.00	0.01
Fe_2O_3/Al_2O_3	1.40	0.40	0.15	0.27	0.21	0.27	0.47	0.12	7.34	0.33	0.25	0.03	0.09	0.25

Fms. formations, *Mems* members, *Jam* Jamuni, *car* carbonate, *Roh* Rohini, *Ban* Bandai, *Dho* Dhorisagar, *Sst* sandstone, *Shl* shale, *Ferr.* ferruginous, *Lat.* latitude, *Long.* longitude, *TOC* total organic carbon

and 3S). Each 0.25 grams of the samples were placed into Teflon beakers and digested with few drops of deionized water and concentrated acids, beginning with 7 ml of concentrated HF (23 M), followed by 3 mL of HNO_3 (15.5 M) and 1 mL of $HClO_4$ (11.57 M). Each sample was finally dissolved in the 10 mL of 1:1 volume of HNO_3 and water and beakers heated over the hot-plate. Several ramping and holding cycles of acid treatment took the samples to dryness. After dryness was attained, samples were again dissolved in the HF. Twenty internal rock standard solutions were prepared similarly and analyzed simultaneously to check analytical quality control of the data.

4 Results

4.1 Petrography

Prior to the petrographic study, fresh samples collected from the field were cleaned with the deionized water and finally air dried in an oven for megascopic study. Summarized megascopic characters (Table 1) and polished surface photographs (Fig. 2) of major litho-units show that the Sonrai Formation comprises of dark grey laminated shale, light grey dolomite, and ferruginous sandstone, whereas, the Solda Formation consists of light grey laminated shale. The dominant rock type in this area is brick-red phosphatic breccia with randomly oriented poorly sorted angular silty phosphatic shale. Besides this, detrital monocrystalline, rounded to sub-rounded poorly sorted quartz and chert clasts, quartzite, and vein-quartz fragments were noticed. Roy et al. (2014) observed that thin sections of highly jointed, moderately fractured siliceous buff phosphatic breccia of Rohini member show encrustations of secondary apatite. The phosphatization of mineral grains is prolific and represented by silty phosphatic shale fragments as well as phosphate cement. It also replaces authigenic silica at several places. The veins and veinlets cutting across the bedding plane at several places. Dark brown, highly ferruginous, coarse-grained, fibrous apatite in the form of encrustations developed over the grain surfaces. The chloritic shale member comprises of alternate bands of dark metapelite and light silty

Table 3 Trace elements (ppm) abundance in clays (< 2 μm fraction) associated with the Bijawars of the Sonrai basin compared to crustal abundance (Mason and Moore 1982)

Fms.	Sonrai										Solda				Crustal abundance
Mems.	Jam. carb.	Gor. shl.			Roh. carb.			Ban. sst.			Chl. shl.			Dhor. shl.	
Samples	GKT17	GKT18	GKT14*	M5	TDB14*	TDB16*	ST10*	TDB9*	PDB7*	M7*	M4*	TDB8*	PDB6*	GKT8	
Cs	0.5	0.5	0.5	0.5	**5.9**	2.1	0.5	0.5	0.5	**3.7**	**4.3**	1.5	2.9	0.9	3
Rb	20	6	3	2	**102**	25	9	10	9	**94**	**142**	**96**	89	45	90
Ba	24	35	**514**	24	**1924**	**896**	26	15	**492**	120	**464**	319	206	151	425
Pb	8	12	6	**21**	**20**	**38**	**16**	**17**	**25**	**40**	**14**	12	**37**	5	13
Sr	10	2	3	3	75	44	34	14	21	15	38	16	40	29	375
La	11.1	1.7	3.4	9	27.6	8	1.3	15.3	5.8	12.3	23.3	17.6	28.2	8.1	30
Ce	21.4	3.4	6.7	15.7	51.2	15.6	1.9	27.7	10	19.8	44.2	31.1	49.1	16.5	60
Pr	2.65	0.72	0.86	2.26	6.39	1.88	0.24	3.32	1.42	2.38	5.64	3.73	5.53	1.96	8.2
Nd	10.4	3.7	3.1	9.2	24.7	7	0.9	12.2	6.7	8.4	22.4	12.8	19.8	6.7	28
Sm	2.3	1.2	0.5	2.2	4.3	1.3	0.1	2.3	2.4	1.8	5.6	2.3	3.7	1.3	6.0
Eu	0.45	0.32	0.06	0.51	0.74	0.38	0.05	0.56	1.1	0.62	**1.55**	0.59	0.71	0.42	1.2
Gd	2.3	1.6	0.5	2.4	3.7	1.1	0.2	2.3	4	2.8	**6.1**	1.7	2.5	2.1	5.4
Tb	0.4	0.2	0.1	0.4	0.6	0.2	0.1	0.4	0.5	0.6	1.2	0.3	0.4	0.4	0.9
Dy	2.1	1.4	0.4	2.4	4	1	0.3	2.8	2.2	3.8	**6.9**	2.2	2.6	2.2	3.0
Ho	0.4	0.3	0.1	0.5	0.9	0.2	0.1	0.6	0.4	0.8	**1.3**	0.5	0.6	0.4	1.2
Er	1.1	0.8	0.3	1.4	2.8	0.6	0.2	1.6	0.8	2.5	**3.5**	1.3	1.7	1.2	2.8
Tm	0.14	0.12	0.05	0.2	0.4	0.09	0.05	0.23	0.1	0.37	**0.51**	0.2	0.25	0.17	0.5
Yb	0.9	0.7	0.3	1.3	2.5	0.6	0.2	1.5	0.5	2.6	3.4	1.5	1.7	1.1	3.4
Lu	0.14	0.11	0.07	0.2	0.38	0.09	0.04	0.23	0.08	0.43	**0.56**	0.25	0.28	0.18	0.5
Y	11	8	3	17	29	7	4	16	10	22	32	10	15	14	33
Th	3.3	2	0.8	4.9	**13.1**	3.6	0.3	5.4	0.6	**9.8**	**9.9**	1.5	**7.4**	2.6	7.2
U	1.4	0.9	0.8	1.5	**8.6**	**2.7**	**2.7**	**2.9**	**2.7**	**2.6**	**4**	1.5	**18.1**	1.4	1.8
Zr	49	29	**411**	57	160	54	24	143	48	162	**224**	66	110	106	165
Hf	1	0.3	**10.8**	1.2	**4.3**	1.1	0.2	**3.6**	0.8	**4.2**	**6**	1.8	2.7	1.9	3
Cr	**120**	90	20	**110**	**220**	70	20	**1030**	**110**	**210**	**250**	**460**	**120**	80	100
V	48	44	17	132	**190**	78	33	37	42	**229**	**195**	**193**	**166**	123	135
Sc	7	3	1	10	9	6	2	5	4	**33**	**37**	**49**	22	14	22
Ni	40	**80**	20	**210**	40	40	20	20	50	**90**	**110**	40	30	30	75
Co	9	6	5	21	8	17	1	3	15	**49**	**39**	5	**83**	**42**	25
Cu	**60**	**80**	**100**	**220**	**80**	**150**	20	50	50	**150**	**100**	30	**100**	**80**	55
Zn	**90**	**410**	**130**	**760**	**250**	**500**	60	**140**	**210**	50	**250**	50	30	**80**	70
Ga	5	3	2	**16**	15	6	1	6	2	**22**	**26**	**27**	**18**	12	15

Table 3 continued

Fms.	Sonrai										Solda				Crustal abundance
Mems.	Jam. carb.	Gor. shl.			Roh. carb.			Ban. sst.			Chl. shl.			Dhor. shl.	
Samples	GKT17	GKT18	GKT14*	M5	TDB14*	TDB16*	ST10*	TDB9*	PDB7*	M7*	M4*	TDB8*	PDB6*	GKT8	
Calculated parameters															
ΣLREE	47.85	10.72	14.56	38.36	114.19	33.78	4.44	60.82	26.32	44.68	101.14	67.53	106.33	34.56	–
ΣHREE	7.48	5.23	1.82	8.8	15.28	3.88	1.19	9.66	8.58	13.9	23.47	7.95	10.03	7.75	–
ΣREE	55.78	16.27	16.44	47.67	130.21	38.04	5.68	71.04	36	59.2	126.16	76.07	117.07	42.73	–
δCe	0.91	0.71	0.90	0.80	0.89	0.93	0.78	0.90	0.80	0.84	0.89	0.89	0.91	0.96	–
δEu	0.92	1.09	0.57	1.05	0.87	1.50	1.66	1.15	1.67	1.30	1.25	1.41	1.10	1.20	–
$(La/Yb)^N$	0.91	0.18	0.84	0.51	0.81	0.98	0.48	0.75	0.86	0.35	0.51	0.87	1.22	0.54	–
Zr/Hf	49	96.7	38.1	47.5	37.2	49.1	120	39.7	60	38.6	37.3	36.7	40.7	55.8	–
Y/Ho	27.5	26.7	30	34	32.2	35	40	26.7	25	27.5	24.6	20	25	35	–
V/V + Ni	0.31	0.17	0.24	0.19	0.64	0.42	0.38	0.40	0.24	0.48	0.39	0.64	0.67	0.60	–
V/Cr	0.29	0.36	0.62	0.88	0.63	0.82	1.21	0.03	0.28	0.80	0.57	0.31	1.01	1.13	–

Concentrations marked with bold letters show enrichment

Ban. sst. Bandai sandstone, *Chl. Shl*. Chloritic shale, *Dhor. shl*. Dhorisagar shale, *Gor. shl.* Gorakalan shale, *Jam. carb.* Jamuni carbonate, *Roh. carb*. Rohini carbonate, *Fms*. formations, *Mems.* Members. * samples from the mineralized zone, *Eu* Europium, *Ce* Cerium, *(La/Yb)* Chondrite normalised (Lanthanum vs. Ytterbium), *N* normalised, *LREE* light rare earth elements, *HREE* heavy rare earth elements

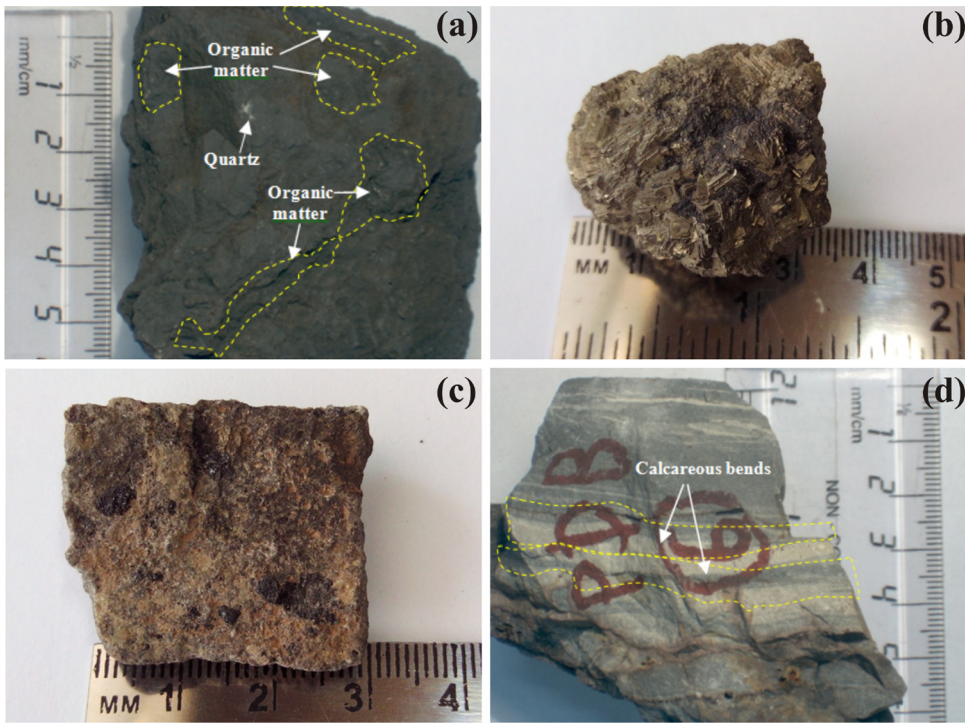

Fig. 2 **a** Gorakalan graphitic shale, **b** pyrite nodules with bitumen from Rohini carbonate, **c** Rohini carbonate with bituminous organic matter and **d** Chloritic shale with calcareous bands

arenaceous bands. Former consists of recrystallized aggregates of muscovite porphyroblasts, whereas, later comprises of quartz clasts. Pyrite and chalcopyrite occupy interstices of clasts and carbonaceous globules.

4.2 XRD

XRD data revealed the dominance of Kln > Chl > Ill > Sm in the Sonrai and Kln > Ill > Chl in the Solda Formations, respectively (Fig. 1S). Clay mineral assemblages for Gorakalan graphitic shale, Rohini carbonate and Bandai sandstone of the Sonrai Formation represent Kln > Chl > Sm, Kln > Sm > Ill > Chl and Kln > Ill > Sm > Chl, respectively. Chloritic shale and Dhorisagar member of the Solda Formation exhibits clay in order of their relative abundance as Kln > Ill > Chl and Ill > Chl > Kln.

4.3 SEM–EDS

Obtained SEM images show a variety of microstructural attributes of the clay minerals (Fig. 3). Based on major oxide data (as an electronic supplement: Tables 1S), structural formulae (Tables 4S and 5S) were calculated for individual clay minerals. Calculated thermodynamic data (Table 4S) when plotted over ternary [M^{+}–4Si–R^{2+}] diagram (Meunier and Velde 1989), data plots lie within the mixed layer field (Fig. 4). Further, octahedral (Zo) versus interlayer (Zt) charges, tetrahedral (Zt) versus octahedral (Zo) charges and tetrahedral (Zt) versus interlayer (Zi) charges (Tables 1S), when plotted over binary diagrams, the data plots confine to illite and chlorite fields (Fig. 5). These data plots show closeness with the data published by Alexandre et al. (2005) for the Dawn and Rabbit lakes and McArthur River basement-hosted unconformity-type deposits of the Athabasca basin.

Based on Si position occupied in the tetrahedral sheet and relative Fe or Fe/(Fe + Mg) values of the octahedral sheet, chlorites of the Sonrai basin were grouped into clinochlore, talc-chlorite, pennantite, ripidolite, and thuringite types. They lie within their compositional limits (Fig. 6). The clinochlore and Mg-chlorite compositions from Rohini carbonate indicate hydrothermal alteration possibly linked to the Kurrat volcanic activity. The Mg rich-chlorite was abundantly found in the alteration zone. Nutt (1989) reported chlorite with high Mg and $Al^{(VI)}$ contents associated with the extensive chlorite dominated alteration zone enclosing an unconformity-type ore body in the Jabiluka U deposit. The U minerals are commonly associated with Mg-rich (e.g. amesite and clinochlore) chlorite and considered the abundance of clay-size Mg-rich chlorite as the end product of alteration. When Fe/(Fe + Mg)$^{2+}$and Si^{+4} values plotted for chlorite compositions (Table 1S), they lie close to the chlorite compositional field of Jabiluka UTUD, Australia (Fig. 7).

4.4 Geochemistry

Despite intensely and hydrothermally altered illite and chlorite associated with the mineralized Rohini carbonate, the Bandai sandstone and Chloritic shale of the Sonrai

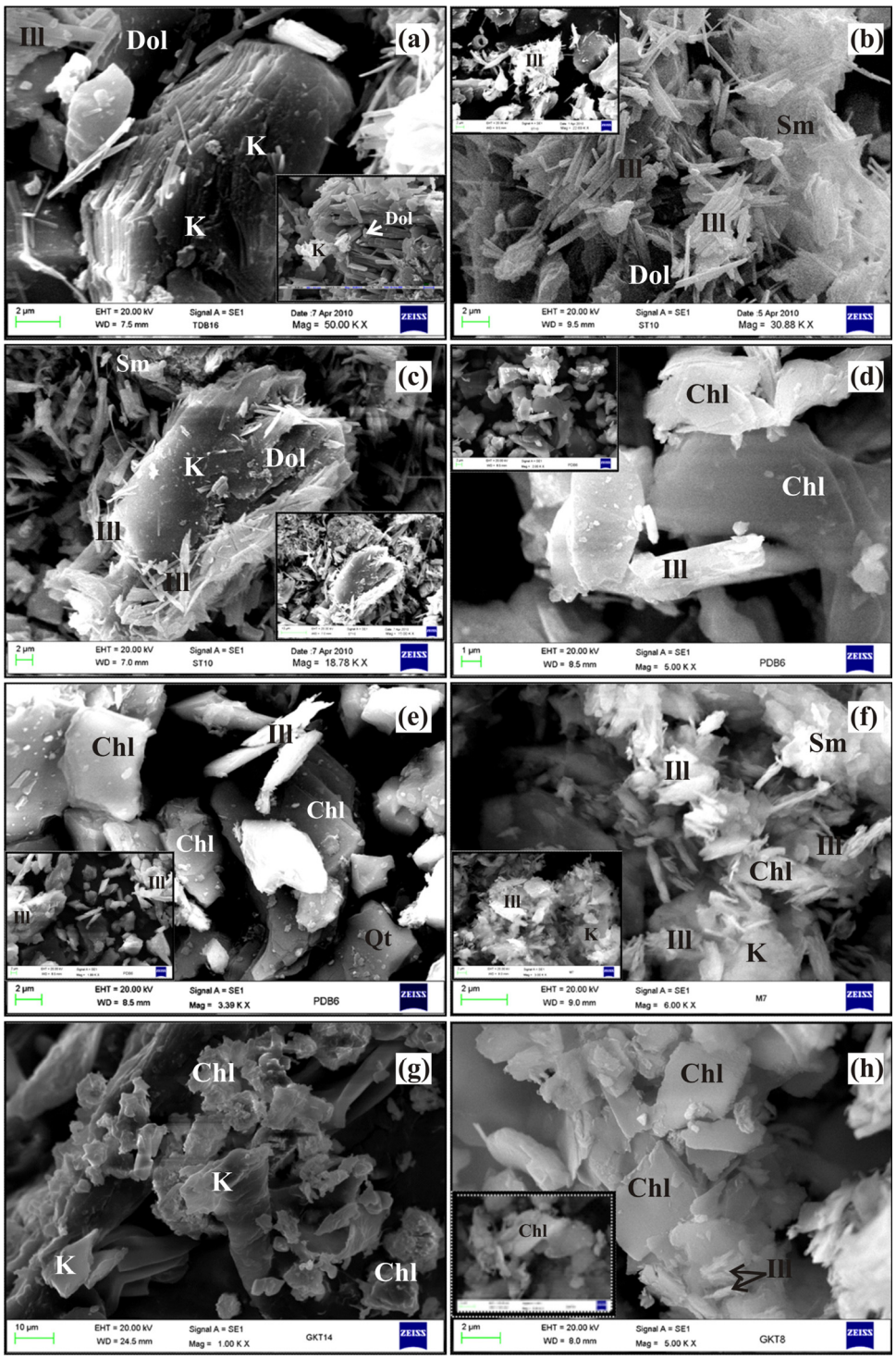

Fig. 3 SEM-BSE images of (1) Rohini carbonate shows **a** platy kaolinite and fibrous, spiky tv-1M poly type illite (in the inset), shattered massive dolomite grains and quartz with flaky kaolinite, **b** abundant needle-shape tv-1M poly type illite (in the inset), shattered massive grains of dolomite and hairy illite **c** display alteration and transformation of kaolinite into hairy tv-1M polytype illite. (2) Chloritic shale shows **d** uneven, flat surface, layered chlorite, massive quartz grains, laths of illite (also seen in the inset), **e** pseudo-hexagonal, platy laths of chlorite and platy illite (in the inset), illite laths and massive quartz gains, (3) Bandai shale shows **f** platy laths of kaolinite, illite, and smectite, (4) Goralalan shale shows **g** platy kaolinite and chlorite and (5) Dhorisagar shale shows **h** uneven, flat surface, layered chlorite and platy flakes of illite (in the inset) platy chlorite and illite

basin show least alteration. PAAS normalized (Nance and Taylor 1976; Taylor and McLennan 1985; Mclennan 1989, 2001) trace elemental data (Table 3) plotted for Gorakalan shale, Rohini carbonate, Bandai sandstone of Sonrai Formation, and Chloritic shale of Solda Formation (Fig. 2S) show large-ion lithophiles (LIL) enrichment. Rb, Ba, Sr, Th, and U in rock units of both the formations indicate high retention of these elements (Fig. 2S). PAAS-normalized REE data when plotted for (a) Jamuni carbonate and Gorakalan shale (b) Rohini carbonate and Bandai sandstone of Sonrai Formation and (c) Chloritic shale and Dhorisagar shale of the Solda Formation (Fig. 8) show low LREE and high HREE abundances. Most of the REE patterns are linear and flattened without any intensive

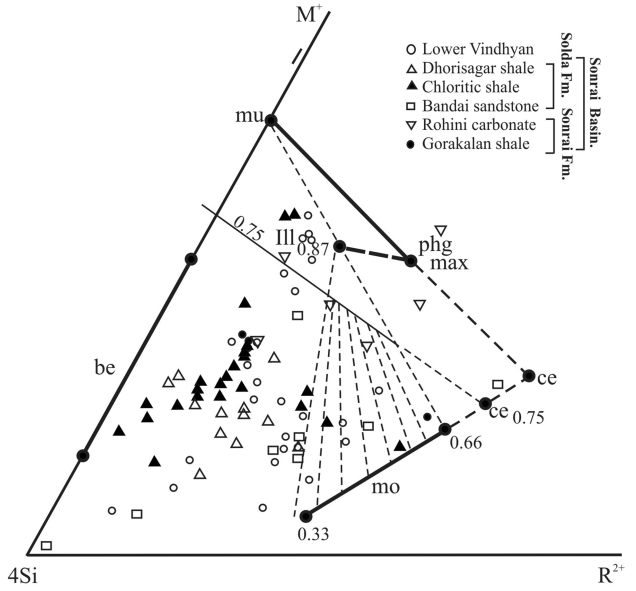

Fig. 4 Chemographic representation of smectites, I/S mixed layers, illite and mica in the M^{+}–4Si–$R2^{+}$ system (after Meunier and Velde 1989) showing data plots (for Solda, Sonrai Formations, and Vindhyan clays) lie within illite and mixed layer clay fields. Bipole solid solutions are represented by heavy lines. Solid-solution tie lines for I/S mixed-layer mineral series are symbolized by dashed lines. *Ce* celadonite, *be* bentonite, *mu* muscovite, *mo* montmorillonite

fractionation (Fig. 8). PAAS-normalized REE patterns show HREEs enrichment, whereas, LREEs represent depletion due to their fractionation (Fig. 9). To study UTUD, Fayek and Kyser (1997) used Post-Archean Australian Shale (PAAS) and Chondrite normalized data plots. REE study on U deposit and their host rocks help to understand genesis and formation of U deposits (Rene 2008; Mercadier et al. 2011). PAAS normalized (Mclennan 1989) REE data (Table 1) plots (Fig. 8) for (a) Jamuni carbonate and Gorakalan shale (b) Rohini carbonate and Bandai sandstone of the Sonrai Formation, and (c) Chloritic and Dhorisagar shale of the Solda Formation, contain low LREE and high HREE values and show linearly/flattened patterns. But Chondrite normalized (Taylor and McLennan 1985) REE data plots show LREEs enrichment and negative Eu anomalies (Fig. 10).

4.4.1 Whole rock geochemical analysis

Out of 14 samples, 10 from Sonrai and 4 from Solda Formations (covering each member) were analyzed for major (Table 2) and trace (Table 3) elemental concentrations by Fusion ICP-MS method. The SiO_2 versus (a) TiO_2, (b) Al_2O_3, (c) $Fe_2O_{3\ (t)}$, (d) Na_2O, (e) CaO and (f) MgO data plotted (Fig. 11) for Jamuni carbonate, Gorakalan shale, Rohini carbonate, Bandai sandstone, Chloritic shale, and Dhorisagar shale units. Besides this, Al_2O_3 versus (a) MgO, (b) Na_2O, (c) K_2O, (d) TiO_2, (e) P_2O_5 and (f) $Fe_2O_{3(t)}$ data also plotted for these units (Fig. 12). High SiO_2, CaO, and MgO contents show positive trends (Fig. 11) for TiO_2 and Al_2O_3 in case of Jamuni carbonate containing abundant smectite and illite phases (Das and Haake 2003). The Gorakalan shale shows linear trends over SiO_2 versus CaO, MgO and Fe_2O_3 diagrams (Fig. 11c, e, f) and Al_2O_3 versus K_2O and P_2O_5 diagrams (Fig. 12c, f). For graphitic shale, the positive correlations between SiO_2 versus TiO_2 and Al_2O_3 (Figs. 11 and 12) show a high degree of weathering which was responsible for the dominance of residual fine clay minerals in this unit. In the case of the Dhorisagar shale of the Solda Formation, the data plotted (Fig. 11) between SiO_2 and Al_2O_3, TiO_2, Fe_2O_3, and Na_2O show high values. High K_2O/Na_2O values (> 2) were found in the case of Gorakalan shale and Rohini carbonate. However, low K_2O/Na_2O values (0.01–2) observed in the case of Jamuni carbonate, Bandai sandstone, and Chloritic shale. The Gorakalan shale shows strong negative anomalies for Rb and Sr and positive anomalies for Pb, Ni, and Zn (Fig. 1Sa).

4.4.2 Altered rock geochemical analysis

The Rohini carbonate shows negative trends over SiO_2 versus CaO, MgO and Na_2O diagrams, however, Fe_2O_3 and TiO_2 data plots (Figs. 11 and 12) representing positive trends, and Fe and Ti enrichment in the residual rocks at the time of chemical weathering. Bandai sandstone show both positive and negative correlations between TiO_2 and Al_2O_3, and Fe_2O_3 and Na_2O data plots (Fig. 11), respectively. The Chloritic shale of Solda Formation is characterized by positive and negative trends as observed in the case of SiO_2 versus Al_2O_3, Na_2O and MgO, Fe_2O_3, TiO_2 data plots (Fig. 11), respectively. The U mineralization reported from Rohini carbonate and Bhandai sandstone from the Sonrai Formation show Eu enrichment which is possibly attributed to reducing environment. Moreover, hydrothermally altered rocks of the Rohini carbonate show M-shaped (Fig. 10) Gd–Tb–Dy–Ho tetrad effect (Masuda et al. 1987) and is more or less similar to that reported from the Moldanubian U deposits (Rene 2008). The mineralized rock of Rohini carbonate (Zr = 160 and Y = 29), Bandai sandstone (Zr = 162 and Y = 22) of the Sonrai Formation and Chloritic shale (Zr = 224 and Y = 32) of Solda Formation represent high mobility of Zr and Y with respect to HREE. Further, high mobility of Zr and Y is explained by M-shaped tetrad effect, accompanied by anomalous behavior of Y, Zr, and Hf. In Bijawar metasediments, non-chondritic Y/Ho and Zr/Hf values (Table 3) vary from 38.1–96.7 to 20–40, respectively. Moreover, these values are comparable to those reported by Rene (2008) from the Rozna and Moldanubian U deposits and suggested considerable mobility of Zr during U mineralization.

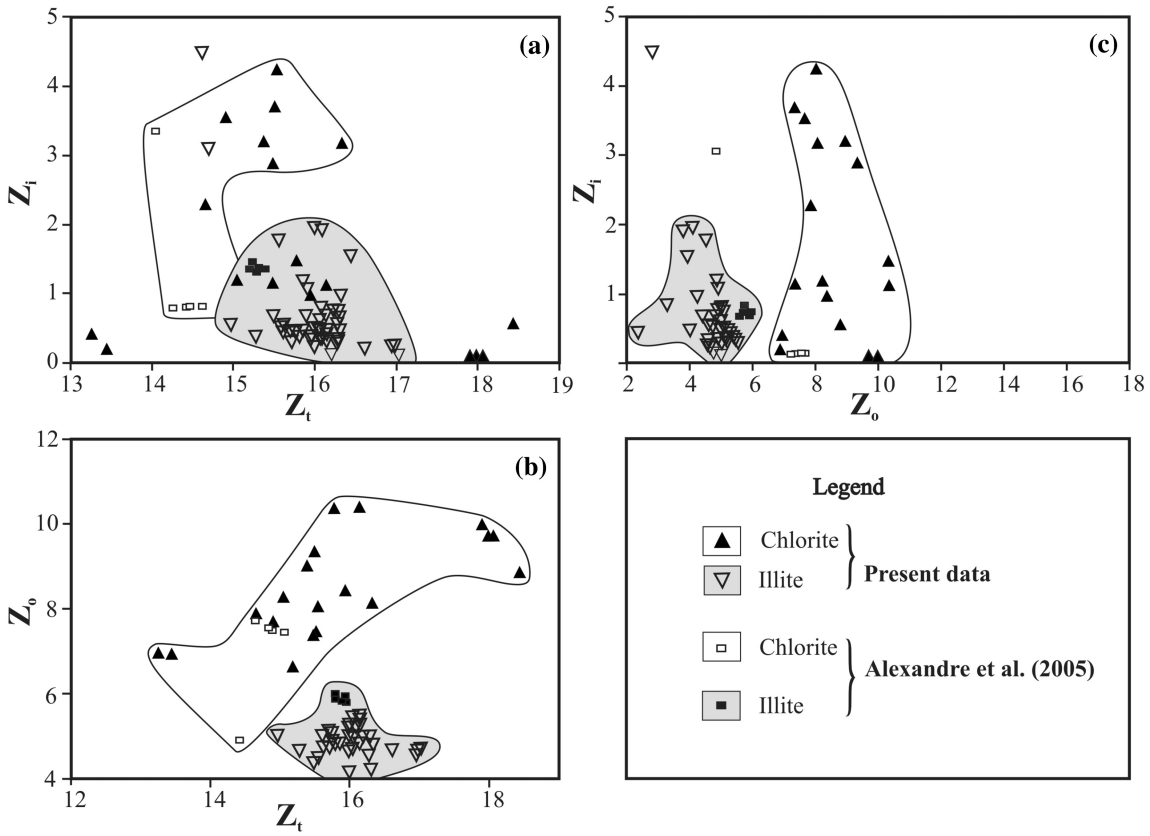

Fig. 5 Bivariate data plots for **a** octahedral (Zo) versus interlayer (Zi), **b** tetrahedral (Zt) versus octahedral (Zo), and **c** tetrahedral (Zt) versus interlayer (Zi) charges in illite and chlorite clays from Sonrai basin (Table 2S) and their comparison with the published data (cited Table 2: Alexandre et al. 2005)

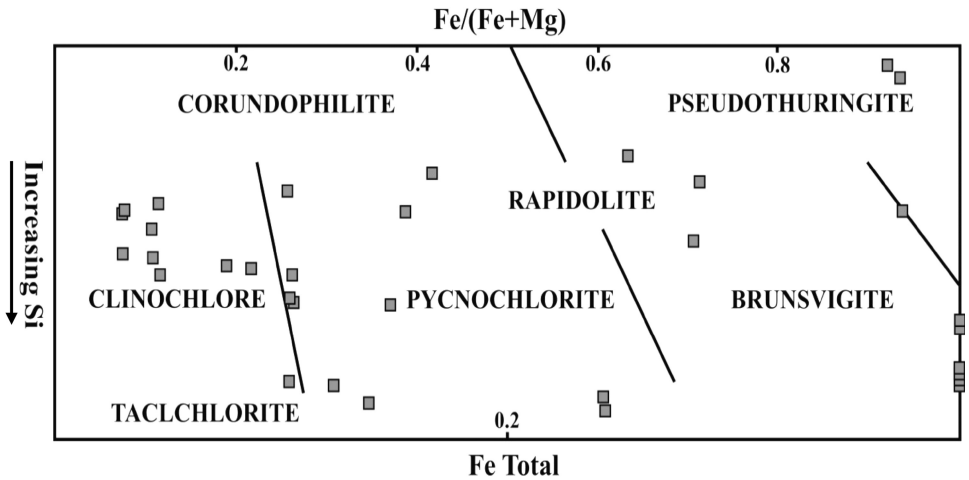

Fig. 6 Chlorite compositions when plotted over Si and octahedral Fe, and Fe/(Fe + Mg) contents (Hey 1954) show clinochlore, rapidolite, talcchlorite and compositions

5 Discussion

In most of the deposits, U precipitation is related to decrease in the oxygen fugacity as resulted from interaction of oxidized U-bearing fluids with reducing agents (Cuney 2009). Common reducing phases include pyrite and buried organic matter. In the Rohini Carbonate, pyrite and chalcopyrite occupy interstices of clasts along with the carbonaceous globules. Iron releases during pyrite oxidation. On the basis of the close temporal and spatial association of U ore bodies with hematite, Alexandre et al. (2005) discussed Fe^{2+} as a potential reducing agent for U^{6+} in UTUD. For precipitation of U^{4+}, inorganic reducing agents include H_2S and Fe^{2+} were derived from pyrite (Cheney 1985; Ruzicka 1993), other Fe-sulfides (Bray et al. 1982) and also from the silicate alteration (Acevedo and

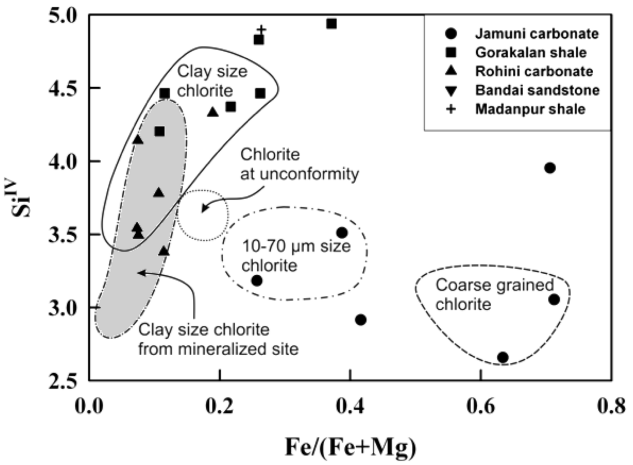

Fig. 7 Present chlorite data when plotted between Fe/(Fe + Mg) and Si (in mole fractions) diagram (Nutt 1989) show compositional correlation with the coarse grained chlorite, 10–70 μm size chlorite, and clay size chlorite from the mineralized zone of Jabiluka UTUD, Australia

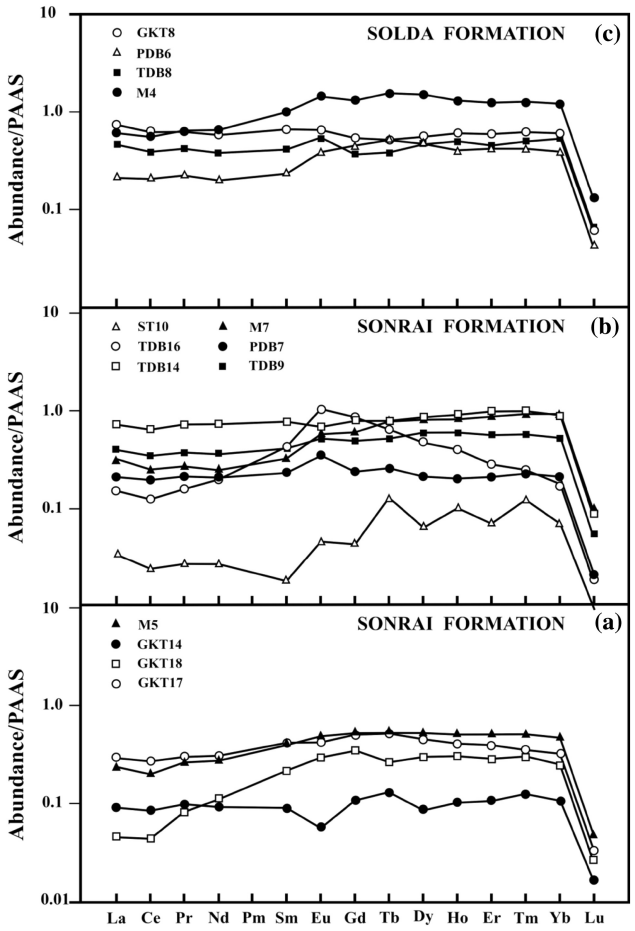

Fig. 8 PAAS-normalized (McLennan 1989) REE (arranged in order of increasing ionic radii) data plots for **a** Jamuni carbonate and Gorakalan shale, **b** Rohini carbonate and Bandai sandstone of Sonrai Formation, and **c** Chloritic shale and Dhorisagar shale of Solda Formation of the Bijawar Group. U mineralization is associated with the Rohini carbonates and Bandai sandstone, whereas other units are non-mineralized

Kyser 2015), respectively. U bearing fluids when coming in contact with the Fe-rich chlorite alteration zones led to simultaneous precipitation of uraninite and hematite (Alexandre et al. 2005). For this area, organic carbon is also considered as one of the significant reducing phases for the removal of U from the solution as carbonate from ore zones also contains a certain amount of organic carbon. U ions possibly transported in the solution in the oxidation state as oxy-ions, although, the possibility of transport of these ions as organic complexes cannot be ruled out. The remobilization and re-precipitation of these ions under redox conditions contributed to redistribution of ore at the time of their formation. Heat supplied by basic igneous activity (Kurrat volcanics) associated with the lower units of the Sonrai Formation was perhaps responsible for remobilization and concentration of the U. Thus, thermal heat supplied by acid and basic magmatism is one of the causes for the multistage remobilization of U in the area. Basic volcanic activity during Bijawar sedimentation is evidenced by the presence of pillow lavas of the Kurrat volcanics (Kumar and Singh 1978). Chemical composition of sedimentary rock primarily depends upon depositional processes (including source rock weathering and sorting), tectonics and paleoclimatic conditions available at the time of their formation (Crichton and Condie 1993; Bauluz et al. 2000). Jha et al. (2012) interpreted clay stratigraphic records in terms of paleoenvironmental conditions and hydrothermal processes. The Sonrai Formation represents Kln > Chl > Ill > Sm mineral assemblages, whereas, Solda Formation contains Kln > Ill > Chl. Former mineral assemblage resulted from alteration process and follow progressive paleoenvironmental (tropical humid to semi-arid/arid cycles) changes that prevailed during maturation of the Sonrai basin. Hydrothermal activity associated with the Kurrat volcanics during reactivation of the rift was accountable for high degree of illitization (Jha et al. 2012). Present U mineralization is restricted to the Rohini carbonate, Gorakalan shale, and Bandai sandstone of the Sonrai Formation. Hydrothermal activity associated with the Kurrat volcanics perhaps provided reducing condition conducive to U ion precipitation. Hydrothermally derived illite and chlorite micro-crystals associated with the U deposits show fine plates, lamellae, tubules, and elongated plate-like structures (Beaufort et al. 2005; Laverret et al. 2006) distinguished by their smaller size, low crystallinity, and common inter-stratification of expandable layers, lath-like or flaky morphology and Mg-rich chemical compositions. The Gorakalan graphitic shale with Kln > Chl > Sm assemblage represents a large amount of kaolinite and smectite, formed by intense rock weathering under humid

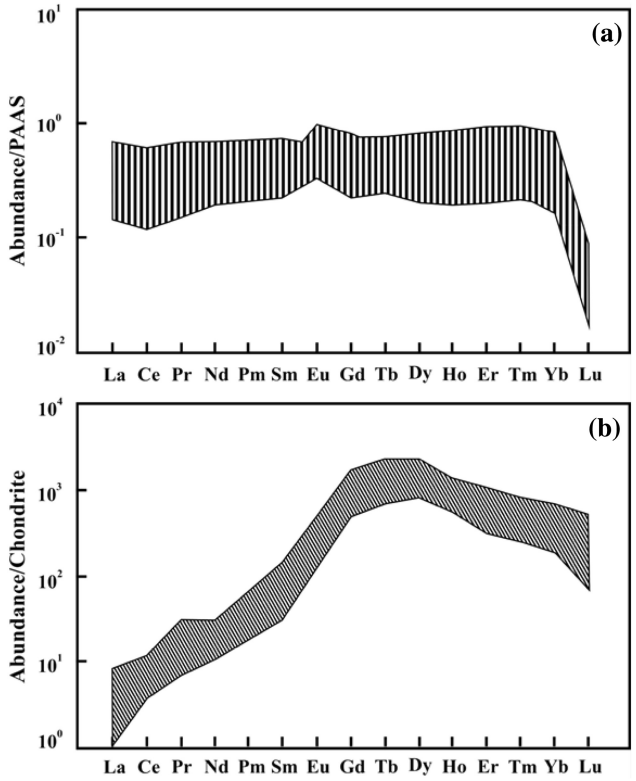

Fig. 9 **a** PAAS normalized (McLennan 1989) REE (arranged in order of increasing ionic radii) patterns for clays (< 2 μm fractions) separated from Rohini carbonate and Bandai sandstone of Sonrai Formation and **b** Chondrite normalized (Anders and Grevesse 1989) REE patterns of the unconformity related McArthur and Sue U deposits of Canada (Mercadier et al. 2011)

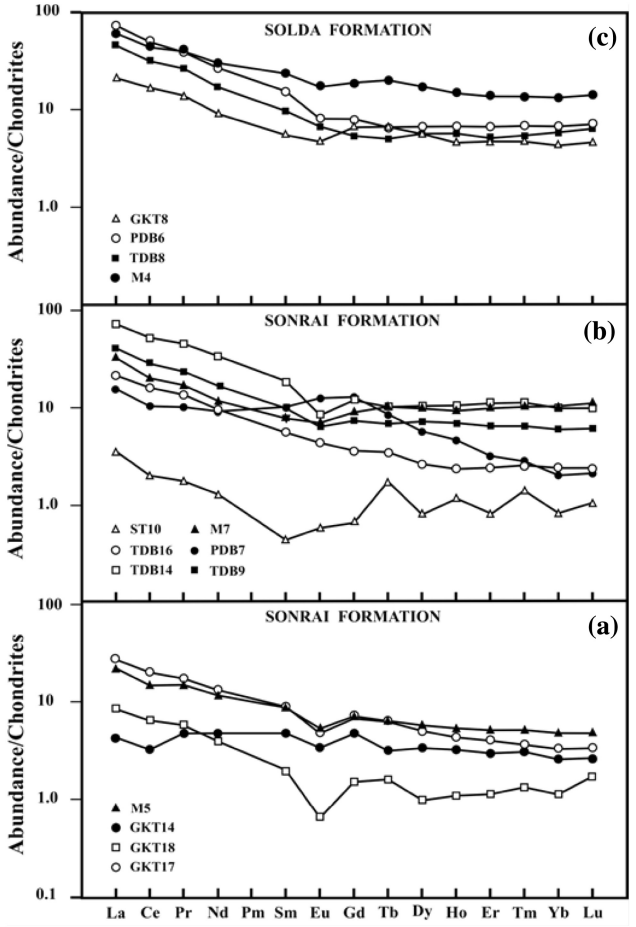

Fig. 10 Chondritic-normalized (Taylor and McLennan 1985) REE (arranged in order of increasing ionic radii) data plots for **a** Jamuni carbonate and Gorakalan shale, **b** Rohini carbonate and Bandai sandstone of Sonrai Formation and **c** Chloritic shale and Dhorisagar shale of Solda Formation of the Bijawar Group

tropical climate. Although, climatic constraints (i.e., tropical weathering) no longer applicable without isotopic data for kaolinite (Thiry 2000). The kaolinite gets converted into illite and chlorite (Hower et al. 1976; Iman and Shaw 1985). Most of the illite converted into chlorite under diagenetic or hydrothermal alterations. The Rohini carbonate contains Kln > Sm > Ill > Chl mineral assemblage and shows hydrothermal alteration and paleo weathering. As a result of K-feldspar and mica leaching from the pre-existing rocks, Si and Al ions produced were required for the formation of kaolinite. Moreover, weathering of granite or basic igneous rocks produces kaolinite (Millot 1970). Thus, the presence of kaolinite is possibly attributed to the leaching and weathering of minerals of these rocks available in the source regions. Bandai sandstone is characterized by Kln > Ill > Sm > Chl assemblage and represents a high degree of illite and chlorite alteration, ascribed to the hydrothermal conditions existed at the time of Kurrat volcanism. The Chloritic shale represents Kln > Ill > Chl assemblage with diagenetic alteration effects on illite and chlorite. The Dhorisagar member contains Ill > Chl > Kln mineral assemblage that shows arid to semi-arid climatic conditions. Moreover, illite and chlorite abundances indicate cold and dry environmental conditions (Singer 1984). Meunier and Velde (2004) discussed that illite is usually derived from the pre-existing K-feldspar rich rocks in arid environments.

REE abundance in the U oxides suggests a type of U deposit (Fryer and Taylor 1987). Fayek and Kyser (1997) discussed that the REE signatures are analogous to the alteration halos associated with the typical UTUD. In the case of U oxides, REE fractionation is important as their ionic radii (1.16 to 0.977 Å) are close to that of U^{4+} (1 Å) in eight-fold coordination. However, most of them are not sensitive to the changes in the redox conditions (Bonhoure et al. 2007). Jha et al. (2012) discussed high fluid/rock interaction and super-saturation of fluids in proximity to the U mineralization.

Chlorite associated with the unconformities and alteration halos represents low Fe/(Mg +Fe) and high Si values. But, clay size chlorite with low Si, Fe/(Fe + Mg) and Al^{vi}/Al^{iv} values suggests chloritization, where, quartz

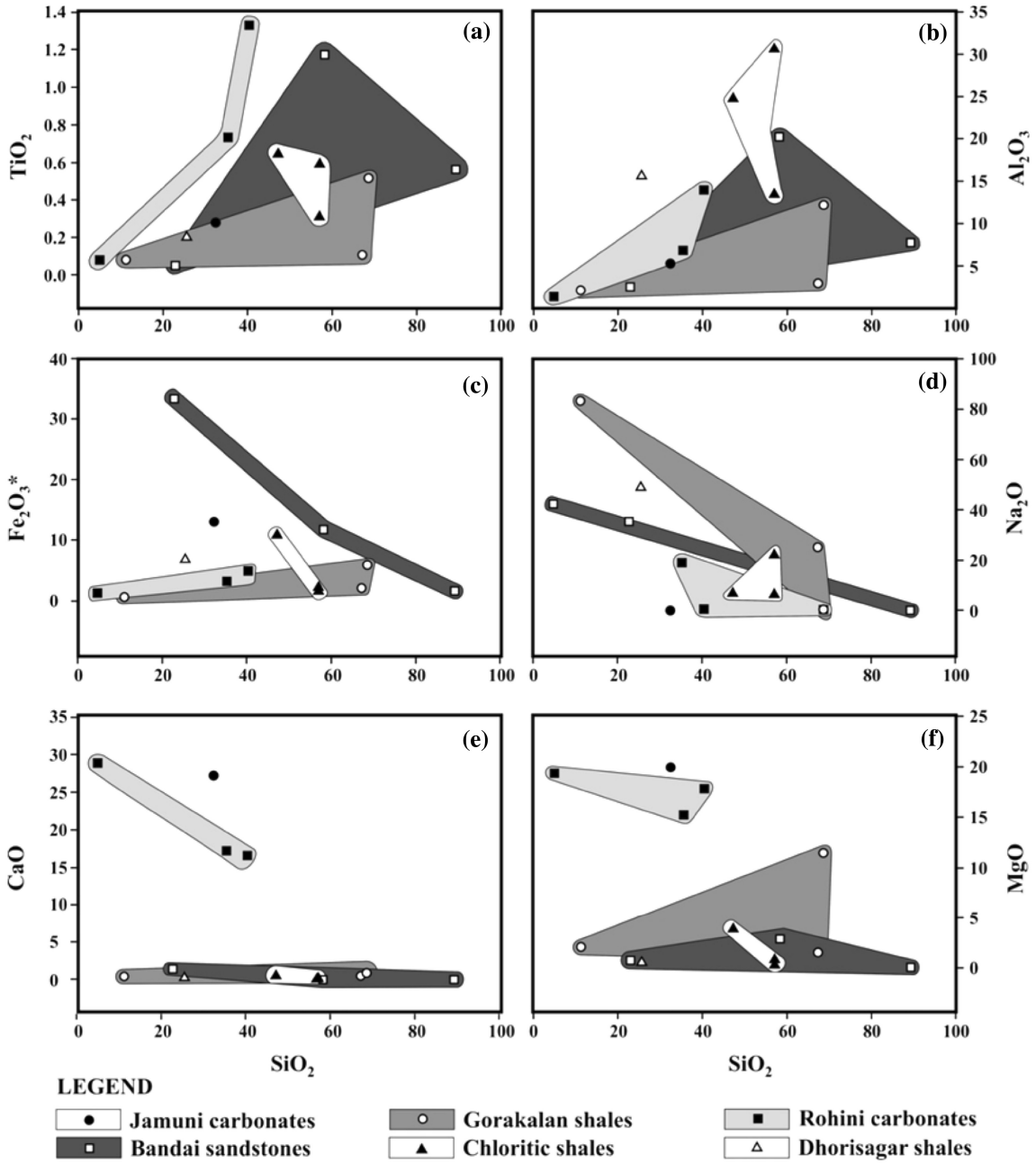

Fig. 11 Bivariate data plots between SiO_2 versus **a** TiO_2, **b** Al_2O_3, **c** Fe_2O_3 (total), **d** Na_2O, **e** CaO and **f** MgO for Jamuni carbonate, Gorakalan shale, Rohini carbonate, Bandai sandstone, Chloritic shale and Dhorisagar shale members of the Bijawar Group

dissolution by Mg-rich fluids at high fluid-rock ratios occurred as a product of alteration (Nutt 1989). The low Fe/(Fe + Mg) values obtained from clay-size chlorite of this area suggest that the Mg-rich fluids were available throughout the process of chloritization. Moreover, chlorite compositional attributes of the Jamuni carbonate resemble coarse-grained chlorite and 10 μm size chlorites of the altered meta-sedimentary rocks (Fig. 7). These coarse-grained chlorites show low octahedral occupancies and also net-layer charges varying from 0.3 - 1.8 and 6.09 - 8.69, respectively (Table 5S). It occurs in veins. These veins cut across the clay-size matrix chlorite. A few Fe and Mg-rich chlorite types contain Mn with negative tetrahedral charges and are restricted to the pennanite and clinochlore compositional fields (Fig. 7). Bailey and Lister (1989 and references therein) discussed that small amount of Ca + Na + K are often reported from chemical analyses of dioctahedral chlorites as cations residing between the 2:1 layers and the interlayer sheet, but they are more likely to be impurities. Amount of K ions present in most of the

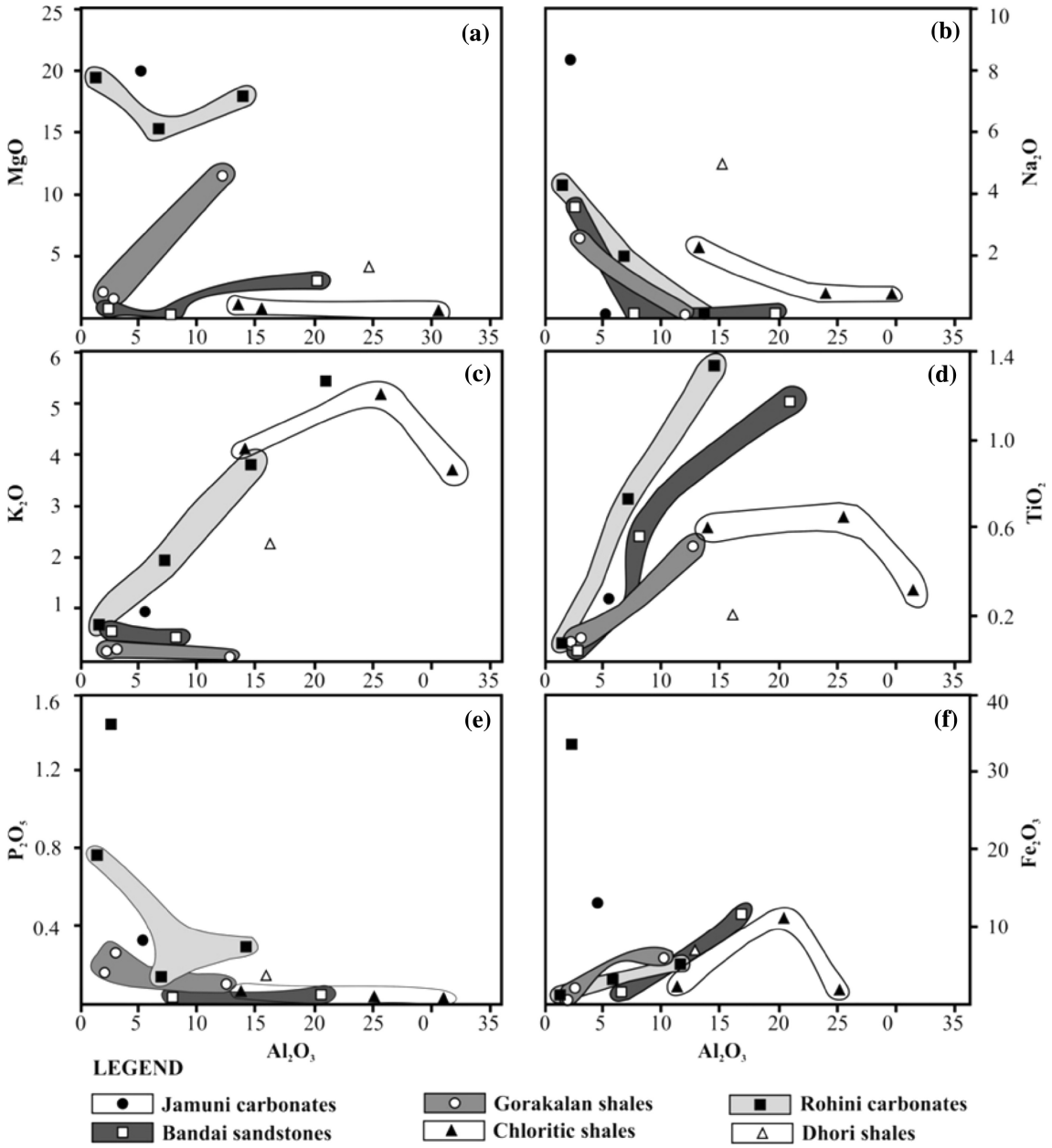

Fig. 12 Bivariate data plots between Al_2O_3 and **a** MgO, **b** Na_2O, **c** K_2O, **d** TiO_2, **e** P_2O_5 and **f** Fe_2O_3 for Jamuni carbonate, Gorakalan shale, Rohini carbonate, Bandai sandstone, Chloritic shale and Dhorisagar shale of the Bijawar Group

chlorites of this area is very close to the K content of chlorite associated with the UTUM (Beaufort et al. 2005). Moreover, hydrothermally altered chlorite contains minor amount (0.01–0.04) of K. Presence of these ions is due to the incorporation of K, Na and Ca ions in the chlorite lattices (Wilkinson et al. 2015). Assumingly, K^+, $Na^{2+}$and Ca^{2+} are present in the mixed-layer chlorite/corrensite (Shau and Peacor 1989). In Jabiluka U deposit, clay-size chlorite is the main constituent of the host rock matrix and is conspicuously associated with the ore minerals. Fine-grained chlorite (ranges from 50 μm in length to < 5 μm across it) appears as cryptocrystalline and categorized as clay size chlorite. Mg-rich host rock alteration mainly involves the exchange of Mg for Fe ions during replacement of the earlier-formed chlorite by clay-size chlorite (Nutt 1989). Chlorite associated with the Gorkalan and Madanpur shale is similar to fine clay size chlorite of the Jabiluka UTUD (as characterized by high Mg and Si contents). Clay size chlorite compositions reflect substitution or replacement in the mineral lattices and a variable degree of chloritization (Nutt 1989). Thus, pre-existing coarse-grained detrital clays so resulted were converted

into authigenic clay size chlorites and characterized by high Si^{4+} and negative tetrahedral charges (including octahedral occupancy that ranges from 1.8 to 4.5). These chlorites contain octahedral Al^{3+} (varies from 1.4 to 2.6), high Mg^{2+} (varies from 1.5 to 3.1) and much higher net layer charges that range from 5.9 to 10.4 (Table 1S). Chlorite composition of the mineralized Rohini carbonate is characterized by high Si^{4+} (3.5) and Mg^{2+} (3%–3.8%) contents with low octahedral occupancy (from 1 to 1.7). The Mg-rich chlorite resembles to clay size clinochlore and sudoites of the Jabiluka U ore deposit (Fig. 7). Most of them formed after mineralization were responsible for U ions remobilization. However, chlorite compositions from Bandai sandstone do not fall within the compositional limit of these chlorites. Present study on clay mineral assemblages or clay-types, paleoclimatic conditions and clay-crystallinities suggested U mineralization in the Sonrai Formation. Presence of clay-size Mg-rich chlorite (Mg-clinochlore) composition of Rohini carbonate suggests early stages of hydrothermal alteration in vicinity of the U mineralization. However, coarse-grained Fe, Al chlorite (pennantite, Al-sudoite, and clinochlore) compositions from Jamuni carbonate and Gorakalan shale show late stages of alteration, occurred far away from the mineralized zone.

Generally, Post-Archaean sedimentary rocks show an increase in the Al_2O_3 versus CaO, Fe_2O_3, MgO and Na_2O ratios with the decrease in the Al_2O_3 versus K_2O ratios (Taylor and McLennan 1985). However, major oxide data do not show their characteristic monomineralic composition as other minerals including quartz, feldspar, dolomite, calcite, and pyrite were also present. None of these clay separates comprised of a single phase, but, they are an admixture of more than one variety of clays, therefore the chemistry of the mixed clay minerals is not comparable to a particular single standard clay mineral. Bivariate data plots (Figs. 11 and 12) show high mobility of Na, Ca, Mg, K, and Fe in almost all the rock units of Sonrai and Solda Formations. The linear trend of CaO and MgO with SiO_2 (Fig. 11) is suggestive of leaching of Ca, Mg, Na, and Fe ions during chemical weathering of the clay minerals (Liu et al. 2009). The high amount of Al, Fe, K, and Mg, but, low Na contents in weathered products of this area is indicative of enhanced chemical weathering as also suggested by Wei et al. (2004). High K_2O/Na_2O values (> 2) found in case of Gorakalan shale and Rohini carbonate is related to periodic upliftment and intense weathering at the time of deposition of these rocks (Sharma and Rahman 2000). However, low K_2O/Na_2O values (0.01–2) associated with the Jamuni carbonate, Bandai sandstone, and Chloritic shale is related to periodic deepening or rifting of the basin (Engel et al. 1974).

Most of the REE patterns are flattened and do not show intensive fractionation (Fig. 10). Owing to the expandable nature of the clay structure, incorporation of a large amount of HREE without fractionation (Fig. 10) is also possible. Cullers and Graf (1983) demonstrated that silicic rocks usually contain high LREE/HREE ratios ad negative Eu anomalies. Therefore, REE patterns of the source rocks are usually preserved in the sedimentary rocks (Taylor and Mclennan 1985; Wronkiewicz and Condie 1989). Although, flat REE patterns with negative Eu anomaly is inherited from the source rock, rich in quartz and silicic feldspar. Cuney (2010) demonstrated REE patterns of uraninite for individual grains from the Dominion reef, South Africa. Duhamel et al. (2009) studies from Elliott Lake show similar characteristics as those associated with the uraninite grains crystallized at high temperature from granite or anatectic pegmatite (such as Rossing, Namibia) includes: (1) almost 104 times more than the chondritic abundance for most of the REE resulted from their increased substitution into the uranium oxide crystals at high temperature compared to those crystallized at lower temperature (Bonhoure et al. 2007). (2) Moderate global fractionation of the REE pattern, reflect a weaker crystalochemical control for REE incorporation relative to their ionic radii into the uraninite structure at high temperature compared to those crystallized at a lower temperature (as shown by comparing to the REE patterns of uranium oxides from unconformity-related deposits). (3) Strong and variable negative Eu anomaly reflects plagioclase fractionation in the magma from which they have been crystallized, similar to the Eu anomalies observed in the uraninite from Rossing and Finland pegmatoids. The phosphatic component is in the form of apatite varying form from microcrystalline to well crystallized coarser crystal aggregates comprised of cement, veins, and botroidal encrustations (Roy et al. 2014). It is generally believed that the Ca is replaced by U, Th, Pb, Fe and REE ions within the apatite lattices and charge imbalance is adjusted through suitable anionic substitution. An important property of apatite is that it accommodates U ions. The mechanism is not completely understood, but most likely it is because of the incorporation of U^{4+} in the apatite mineral structure that replaces Ca ions. The decaying organic material reduces the U^{6+} to U^{4+}, facilitating its incorporation into the apatite structure. More or less similar studies of Stevko et al. (2014) revealed that the fractures and interstitial spaces between fluorapatite crystals were filled-up by younger crystals and aggregates. In context to REE geochemistry of phosphorites of the Sonrai area, where, normalized REE patterns show positive Eu anomalies are attributed to reducing conditions as also inferred earlier by Khan et al. (2012). Moreover, Post-Archean sediments show similar rare earth patterns and characterized by

negative Eu anomalies of almost constant magnitude (relative to chondrites) and nearly constant LREE/HREE values (Nance and Taylor 1976). It occurs due to chemical fractionation of plagioclase feldspar in the continental crust (Taylor and McLennan 1985). Contrarily, continental Eu enriched crust indicates reducing environment eventually evolved in the upper continental crust.

Roy et al. (2004) reported U mineralization from carbonate and sandstones of the Sonrai Formation characterized by marginal Eu enrichment that also in the M4 sample of Solda Formation (Table 3). Overall high (0.35–0.98) La/Yb values are attributed to reducing environmental conditions. PAAS normalized elemental data plots show enrichment of large-ion lithophiles (LILs). Marginal enrichment is noticed in the case of Rb. But, Ba, U, and Th concentrations are as high as > 4, > 10 and > 20 times higher than the crustal abundance (Table 4), suggest enrichment in TDB14, PDB6, and PDB14 specimens, respectively. Adsorption and high retention of U and Th ions are inferred during chemical weathering and diagenesis. Present data show concentrations > 3 and > 4 times higher than the crustal abundance of Pb and Ba, indicating enrichment in the mineralized Bandai sandstone (M7) and Rohni carbonate (TDB14) of the Sonrai Formation clays. It is explained by low mobility as well as retention of these elements on the tetrahedral as well as inter-layer sites of the smectite rich clays under reducing conditions (Balasubramaniam et al. 1989). But, non-mineralized Gorakalan shale shows strong negative (for Rb and Sr) as well as positive (for Pb, Ni, and Zn) anomalies (Fig. 2Sa). Concentrations $\sim$ 2, 4, and 10 times higher than the crustal abundance of Pb, Ni, and Zn show their enrichment, respectively. Such enrichment of cation is accountable for positive anomalies, but, these anomalies are restricted to Gorakalan shale only. But, in general, both Sonrai and Solda Formations represent concentrations > 4 and > 10 times higher than the crustal abundance of Cu and Cr elements suggest enrichment, respectively (Fig. 3S). Such high cationic concentrations are due to their occupancies in the octahedral sites of the illite and smectite structures. Moreover, retention of Cr within the matrix and primary structures of the alumino-silicates at the time of weathering is evidenced by positive Cr anomaly associated with a maximum number of litho-units of this area, although, Cu, Zn, and Pb ions released with ease are absorbed on to fine-grained clays. In general, high Th, U, Sc, Cr, Ni, and V mobility in both the formations indicate acidic environmental conditions that existed during chemical weathering (Fig. 2S). Both Th and U show positive anomalies for most of the Sonrai Formation clays (Fig. 2Sa), but, Th depletion is observed in ST10 and PDB7 samples. REEs, Th, Pb, and Sc contents (Table 3) observed in these rocks is comparable to the crustal abundance (Mason and Moore 1982) as their distribution is least affected by the secondary processes such as diagenesis and metamorphism. Likewise, Zr, Hf, and Sc are also least affected by heavy mineral fractionation. Moreover, enrichment of Pb and Zn in the Sonrai Formation is indicative of anoxic conditions prevailed during deposition (Fig. 3Sa), but, Pb, Mo, Cu and Zn enrichment found in these clays is due to sulfides and organic matter associated with the anoxygenic sediments (Taylor and McLennan 1985). High field-strength elements, such as Zr and Hf show negative correlation for Sonrai and Solda Formation rocks due to their low water solubility and physiochemically resistant to weathering and alteration (Fig. 3S). However, GKT14 (of Gorakalan shale)

Table 4 Summarized trace element concentrations (in ppm) and their enrichment (number of times higher than the crustal abundance) in clay minerals associated with the Sonrai metasediments

Elements	Enrichment	Samples
U	Marginal to > 10	TDB14, TDB16, ST10, TDB9, PDB7, M7, PDB6
Th	Marginal to < 2	TDB14, M7, M4, PDB6
Pb	Marginal to > 3	M5, TDB14, TDB16, ST10, TDB9, PDB7, M7, M4, PDB6
Rb	Marginal	TDB14, M7, M4,TDB8, PDB6
Ba	Marginal to > 4	GKT14, TDB14, TDB16, PDB7, M4
Eu, Gd, Dy, Ho, Er, Tm, Lu	Marginal	M4
Zr, Hf	Marginal to > 3	GKT14, M4
Sc	Marginal to > 2	M7, M4, TDB8
Ni	Marginal to > 2	GKT18, M5, PDB7, M4
Co	Marginal to > 3	M7, M4, PDB6, GKT8
Cu	Marginal to > 4	GKT17, GKT18, GKT14, M5, TDB14, TDB16, M7, M4, PDB6, GKT8
Zn	Marginal to> 10	GKT17, GKT18, GKT14, M5, TDB14, TDB16, TDB9, PDB7, M4, GKT8

and M4 (of Chloritic shale) specimens represent concentration > 3 times higher than the crustal abundance of Zr and Hf, indicating enrichment. Though, these elements were perhaps derived from the granitic basement source rocks. Significantly, Cr, V, and Ni show positive trends, whereas Co and Sc show negative trends for the Sonrai Formation clays, but Ni and Cr show negative correlation for the Solda Formation clays (Fig. 3Sb). These elements not only reside in the clay fractions, but their abundance is also related to clay minerals (Condie 1992). High Ba values in the Rohini carbonate (samples TDB14 and TDB16) and Bandai sandstone (sample PDB7) indicate their adsorption onto clay particles during chemical weathering (Nesbitt and Young 1984).

Further, REE fractionation at the time of chemical precipitation of carbonate is controlled by fixation or supergene enrichment processes; therefore, clays represent high La/Yb values (Zhaoliang et al. 2006). HREE enrichment and LREE depletion in Sonrai and Solda Formations show a high degree of fractionation. Due to high mobility, REE ions occur abundantly during hydrothermal alteration and chemical weathering (Fig. 2S). Mobility, as well as fractionation of REE, is affected by the alteration processes (Nesbitt 1979). As illite, mica, and feldspars are susceptible to alteration; a significant change in the REE patterns is also observed. Rare earth elements were mobilized at the time of incipient and moderate stages of weathering. But, REE ions mobilization was not so during intense weathering. Thus, the former process is more responsible for the mobilization and fractionation of these elements. Fractionation of the REE in these clays is also related to selective leaching of the rocks which contain both stable and unstable minerals. REE ions released from the weathered minerals preferentially and subsequently concentrated to yield supergene enrichments (Middelburg et al. 1986). Fayek and Kyser (1993) pointed out that U bearing minerals possess slightly low total REE contents; therefore, they were not substantially remobilized or fractionated at the time of the alteration. Owing to the fractionation, PAAS normalized REE patterns reflect HREE enrichment and LREE depletion (Fig. 9). To some extent, REE fractionation is also responsible for the shrinking of U oxide structure by crystallization of co-genetic LREE-rich minerals (Gaboreau et al. 2007). Consequently, total REE content decreases and departure is observed in LREE and HREE patterns. It is due to crystallographic control of the mineral structure, thus, display preferential incorporation of HREE having similar ionic radii to U^{4+}, thus, forms HREE enriched patterns as centered from Tb to Er (Fig. 9). PAAS normalized REE patterns of the Rohini carbonate and Bandai sandstone units of the Sonrai Formation (Fig. 9) form asymmetrically HREE enriched patterns. Incidentally, they show a close resemblance to the REE patterns of the McArthur River, Cigar Lake, and Sue Unconformity Type U deposits, Canada (Mercadier et al. 2011). Hydrothermally altered illite and chlorite with a high amount of total REE contents (Table 3) are associated with the mineralized Rohini carbonate, Bandai sandstone, and Chloritic shale of the Sonrai basin (Jha et al. 2012). Thus, high total REE content of the alteration halos is because of the high amount of clays. High HREE content in the bulk composition of these rocks and the high proportion of HREE enriched clays are mutually interrelated. Additionally, weak Ce anomaly suggested high rock-fluid interaction and low fractionation during diagenesis under oxic conditions (German and Elderfield 1990). Oxidization of V forms soluble V^{6+} under oxic conditions and reduced to V^{4+} and form insoluble $VO(OH)_2$ under mildly reducing conditions (Wanty and Goldhaber 1992). Some other redox-sensitive elements such as Co and Cr behaved in a similar manner under oxidizing conditions (Algeo and Maynard 2004). Proportionality of V/Ni is mainly expressed by V/(V + Ni) and is commonly used to find out Eh and pH in the depositional environment (Lewan and Maynard 1982; Madhavaraju and Lee 2009). Low (< 0.46) V/(V + Ni) values in most of the samples pointing towards oxic conditions. Whereas, a few of the values ranging from 0.60 to 0.63 (Table 3) indicate that these sediments were deposited under dioxic conditions. Thus, V is enriched under anoxic conditions (Cao et al. 2012). Clay associated with the Sonrai basin represent (low < 2) V/Cr values, indicating an oxic depositional environment (Kuscu et al. 2016). Comparing to other rocks of this area, Rohini carbonate, Bandai sandstone, and Chloritic shale show high U and Th abundance (Table 3) and also a high degree of REE substitution within their clay complexes. As a result, high total REE and LREE/HREE values found in the clay complexes of the Rohini carbonate, Bandai sandstone of the Sonrai Formation and Chloritic shale, reflect hydrothermal alterations (illitization, chloritization, and carbonatization), perhaps related to Kurrat volcanic activity (Jha et al. 2012). Although, it is quite common that REE patterns normalized to chondrite (Fig. 10) and to PAAS (Figs. 8, 9) and show mutually contrasting patterns (Rene 2008) as former is affected by the extent of tetrad effect (Masuda et al. 1987). Owing to REE mobility variations in F, P, and CO_2 enriched hydrothermal fluids, chondrite-normalized REE patterns show consecutive curved (La–Ce–Pr–Nd; Pm–Sm–Eu–Gd; Gd–Tb–Dy–Ho; and Er–Tm–Yb–Lu) tetrads (Rene 2008) which are either convex or concave, form M-and W shape patterns, respectively (Masuda et al. 1987). Takahashi et al. (2002) also reported similar patterns from the rock-water system of the U ore deposits. Hydrothermally altered Rohini carbonate (sample ST10) shows M-shaped Gd–Tb–Dy–Ho tetrad effect (Figs. 8b and 10b), analogous to that reported from the

Table 5 Range of elemental ratios for Sonrai and Solda metasediments when compared to the trace elemental ratios in similar fractions derived from mafic and felsic rocks, upper continental crust, and Post-Archean Australian Shale

Elem. ratios	Formations		Sediments sources from		UCC***	PASS***
	Sonrai Fm.[1a]	Solda Fm.[1b]	Mafic rocks*	Felsic rocks**		
La/Sc	0.24–1.28	0.33–3.54	2.50–16.3	0.43–0.86	2.21	2.40
La/Co	0.17–2.08	0.16–13.96	1.80–13.8	0.14–0.38	1.76	1.65
Th/Sc	0.33–1.60	0.03–0.37	0.84–20.5	0.05–0.22	0.79	0.90
Th/Co	0.32–2.84	0.10–0.47	0.67–19.4	0.04–1.40	0.63	0.63
Th/Cr	0.04–0.45	0.02–0.46	0.13–2.7	0.018–0.05	0.13	0.13

Data for 1a and b = present study. Data Sources: *, Cullers (1994, 2000); **, Cullers et al. (1988), Cullers and Podkovyrov (2000); ***, Taylor and McLennan (1985)

Moldanubian U deposits (Rene 2008). Lanthanide tetrad effect accompanied by anomalous behavior of Y, Zr, Hf, and other immobile elements is suggestive of significant change in their mobility during alternate oxidation and reduction processes (occurred in the hydrothermally altered carbonate) which led to the precipitation of disseminated U ores (Rene 2008). Such mineralization is associated with the clay minerals and found within or along with the fractures of the Rohini carbonate and Bandai sandstone. Mineralized Rohini carbonate, Bandai sandstone and Chloritic shale (Table 3) represent high Zr and Y mobility with respect to HREE. As a result, Y and Zr rich U ore complexes were formed. High Zr and low Y values are also found in the graphitic Gorakalan shale which is due to unpredictable high Zr mobility during weathering and deposition of the granitic basement (U source rock); however, it was least affected by hydrothermal activity. Positive Eu anomaly (Fig. 8) associated with the Sonrai Formation is explained by the presence of reducing conditions at the time of precipitation of U ions (Mercadier et al. 2011). Abundant sulfide minerals associated with the Rohini carbonate and Bandai sandstone pointing towards reducing conditions. Crystallographic control over mineral composition is influenced by hydrothermal process. In the vein-type U oxides and roll-front type U deposits, rare earth elements are highly fractionated. Obtained La/Sc, La/Co, Th/Sc, Th/Co and Th/Cr values for the clays associated with the Bijawar rocks when compared to felsic and mafic rocks as well as to upper continental crustal (UCC) and PASS values (Table 5) show comparable values to that of the intermediate to felsic source rocks. Most of the U and REE enriched clays in this area are pointing towards their derivation from the fertile Bundelkhand K-feldsphathic granitoid source under oxidizing conditions. Thus, trace elements incorporated in clay minerals signify changes in the physicochemical constraints (such as temperature and composition of the mineralizing fluids) at the time of U ore deposition.

Trace elemental abundance in clay minerals largely depends upon cation interaction with existing crystal structures, ionic radii, electronegativity and crystal field stabilization energy especially in case of transition elements (Rollinson 1993). Thus, clay crystal chemistry is complex with cationic and anionic substitutions being common due to mixed-layer architecture in which two or more mineral structures occur randomly. As diagenesis progresses, the cationic substitution increases in the tetrahedral and octahedral sites that causes changes in the interlayer charges (Nadeau and Bain 1986). Incidentally, Mg and Mg–Fe rich chlorites show close similarity to the diagenetic as well as hydrothermal chlorites (sudoite) of the Jabiluka U deposit, Australia. Few chlorites with low Si (< 3) and high Fe contents (> 0.2) represent low-grade metamorphic effects (Fig. 7). These chlorites are comparable to the chlorite spherules and metamorphic chlorites of the Alligator River U deposits, Australia (Beaufort et al. 2005) and resulted from existing geothermal conditions. Thus, suggesting that the alteration is accountable for the remobilization of U ions.

6 Conclusion

Mineralized Rohini carbonate shows moderate rainfall and reducing conditions, favorable for a high degree of U substitution in the clay lattices. Mineralogical studies together with field evidence revealed that the intense chloritization and illitization were associated with the alteration halos, resulted from progressive fluid-rock interaction processes within the network of active faults and fractures on both sides of the unconformity between the Sonrai metasediments and the metamorphic basement rocks. Low Fe/(Fe + Mg) values obtained for clay-size chlorite suggested that the Mg-rich fluids were available throughout the process of chloritization. Major oxide data show high mobility of Na, Ca, Mg, and K ions which led to Fe and Ti ionic enrichment during chemical weathering of clay minerals. High K_2O/Al_2O_3 and MgO/Al_2O_3 values for the Rohini carbonate and Chloritic shale show intense illitization due to hydrothermal alteration.

PAAS normalized trace elements data plots show U, Th, Rb, Ba, and Sr enrichment, whereas, Bandai sandstone and Rohini carbonate clays show HREE enrichment with asymmetrical patterns, akin to those reported from the well-established McArthur River, Cigar Lake and Sue UTUD of Canada. Chondrite-normalized REE plots form four convex M/W shape consecutive curved tetrads (La-Ce–Pr–Nd, Pm–Sm–Eu–Gd, Gd–Tb–Dy–Ho, and Er–Tm–Yb–Lu) and show evidence of strong water–rock interaction. Hydrothermally altered Rohini carbonate REE data plots show M shape Gd–Tb–Dy–Ho tetrads and anomalous high Y, Z, and Hf contents together with the negative Eu anomalies (associated with the highly altered clays) is suggestive of anoxic conditions. Due to the incorporation of HREE (without fractionation) in the clay interlayer spaces, REE data plots show linear and flattened trends. High U and Th abundances and total high REE content associated with the altered clay minerals of the mineralized Rohini carbonate, Bandai sandstone, and Chloritic shale are related to a high degree of REE substitution within their clay complexes. Moreover, weak Ce anomalies suggest high rock-fluid interaction and low fractionation during diagenesis under oxic conditions. REE and U enrichment in clays indicate derivation of a significant amount of U ions from fertile Bundelkhand granitoid source under oxidizing conditions.

Acknowledgements JPS acknowledges Delhi University for financial support towards this work in the form of R&D Project Grant (No. DRCH/R&D/2012-2013/4155).

References

Acevedo A, Kyser TK (2015) Fe isotopic composition of alteration minerals from mcarthur river zone 4 deposit, Athabasca Basin, Saskatchewan. In: Potter EG, Wright DM (eds) Targeted geoscience initiative 4: unconformity-related uranium systems, open file, vol 7791. Geological Survey of Canada, Ottawa, pp 61–73

Alexandre P, Kyser K, Polito P, Thomas D (2005) Alteration mineralogy and stable isotope geochemistry of Paleoproterozoic basement-hosted unconformity-type uranium deposits in the Athabasca Basin, Canada. Econ Geol 100:1547–1563

Algeo TJ, Maynard JB (2004) Trace element behavior and redox facies in core shales of Upper Pennsylvanian Kansas-type cyclothems. Chem Geol 206:289–318

Anders E, Grevesse N (1989) Abundances of the elements: meteoritic and solar. Geochim Cosmochim Acta 53:197–214

Bailey SW, Lister JS (1989) Structures, compositions, and X-ray diffraction identification of dioctahedral chlorites clays and clay miner. Clays Clay Min 37(3):193–202

Balasubramaniam AS, Phienwej N, Indraratna B, Bergado DT (1989) Predicted behavior of a test embankment on Malaysian marine clay. In: International symposium on trial embankments on Malaysian Marine Clays, Kuala Lumpur, Malaysia, vol 2, pp 1–8

Bao Z, Zhao Z, Guha J, Williams-Jones AE (2004) HFSE, REE, and PGE geochemistry of three sedimentary rock-hosted disseminated gold deposits in southwestern Guizhou Province, China. Geochem J 38:363–381

Bauluz B, Mayayo MJ, Fernandez-Nieto C, Gonzalez Lopez JM (2000) Geochemistry of Precambrian and Paleozoic siliciclastic rocks from the Iberian Range (NE Spain): implications for source-area weathering, sorting, provenace, and tectonic setting. Chem Geol 168:135–150

Beaufort D, Patrier P, Laverret E, Bruneton P, Mondy J (2005) Clay alteration associated with Proterozoic unconformity-type uranium deposits in the East Alligator Rivers Uranium Field (Northern Territory, Australia). Eco Geol 100:515–536

Bonhoure J, Kister P, Cuney M, Deloule E (2007) Methodology for rare earth element determinations of uranium oxides by ion microprobe. Geostand Geoanal Res 31:209–225

Borovec Z (1981) The adsorption of uranyl species by fine clay. Chem Geol 32(1–2):45–58

Bray CJ, Spooner ETC, Golightly JP, Saracoglu N (1982) Carbon and sulphur isotope chemistry of unconformity-related uranium mineralization, McClean Lake deposits, N., Saskatchewan, Canada: Geol Soc of Amer, Abstracts with programs, vol 14, p 451

Cao J, Wu M, Chen Y, Hu K, Bian L, Wang L, Zhang Y (2012) Trace and rare earth element geochemistry of Jurasic mudstones in the northern Qaidam Basin, northwest China. Chem Erde 72:245–252

Cheney ES (1985) Similarities between roll-front and Athabasca unconformity-type uranium deposits and the possible role of sulphides in their origin. In: Sibbald TII, Petruk W (eds) Geology of uranium deposits, CIM Sp vol 32, p 268

Condie KC (1992) Proterozoic terranes and continental accretion in southwestern North America. In: Condie KC (ed) Proterozoic crustal evolution. Elsevier, Amsterdam, pp 447–480

Crichton JG, Condie KC (1993) Trace elements as source indicators in cratonic sediments: a case study from the early Proterozoic Libby Creek Group, southwestern Wyoming. J Geol 101:319–332

Cullers RL (1994) The controls on the major and trace element variation of shales, siltstones and sandstones of Pennsylvanian—Permian age from uplifted continental blocks in Colorado to platform sediment in Kansas, USA. Geochim Cosmochim Acta 58(22):4955–4972

Cullers RL (2000) The geochemistry of shales, siltstones and sandstones of Pennsylvanian-Permian age, Colorado, U.S.A.: implications for provenance and metamorphic studies. Lithos 51:305–327

Cullers RL, Graf J (1983) Rare-earth elements in igneous rocks of the continental crust: intermediate and silicic rocks—ore petrogenesis. In: Henderson P (ed) Rare-earth geochemistry. Elsevier, Amsterdam, pp 275–316

Cullers RL, Podkovyrov VN (2000) Geochemistry of the Mesoproterozoic Lakhanda shales in southeastern Yakutia, Russia: implications for mineralogical and provenance control, and recycling. Precamb Res 104(1–2):77–93

Cullers RL, Barrett T, Carlson R, Robinson B (1987) Rare-Earth element and mineralogical changes in Holocene soil and stream sediment: a case study in the wet mountains region, Colorado, USA. Chem Geol 63:275–297

Cullers RL, Basu A, Suttner L (1988) Geochemical signature of provenance in sand-size material in soils and stream sediments near the Tobacco Root batholith, Montana, USA. Chem Geol 70(4):335–348

Cuney M (2009) The extreme diversity of uranium deposits. Miner Depos 44:3–9

Cuney M (2010) Evolution of uranium fractionation processes through time: driving the secular variation of uranium deposit types. Econ Geol 105:553–569

Daniels EJ, Altaner SP (1990) Clay mineral authigenesis in coal and shale from the Anthracite region, Pennsylvania. Am Mineral 75:825–839

Das BK, Haake B (2003) Geochemistry of Rewalsar Lake sediment, Lesser Himalaya, India: implications for source area weathering, provenance and tectonic setting. Geosci J 7:299–312

Drever JJ (1973) The preparation of oriented clay mineral separations for X-ray diffraction of analysis by a filter membrane peel technique. Am Miner 58:553–554

Duhamel I, Cuney M, Van Lichtervelde M (2009) First characterization of uraninite in an Archean peraluminous granitic pegmatite at Tanco (Manitoba, Canada). Inference for uraninite placer deposits [abs.]: Geological Association of Canada-Mineralogical Association of Canada Conference, Québec, Canada, vol 33, p 50

Engel AE, Itson SP, Engel CG, Stickney DM, Cray EJ Jr (1974) Crustal evolution and global tectonics: a petrogenic view. Geol Soc Am Bull 85:843–858

Fayek M, Kyser TK (1993) Petrography, chemical ages, stable isotopes composition, and REE contents of three stages of uranium mineralization from the Athabasca basin, Saskatchewan. Geol Surv Rep 93(4):8

Fayek M, Kyser TK (1997) Characterization of multiple fluid-flow events and rare-earth-element mobility associated with formation of unconformity type uranium deposits in the Athabasca basin, Saskatchewan. Can Miner 35:627–658

Fryer BJ, Taylor RP (1987) Rare-earth element distributions in uraninites: implications for ore genesis. Chem Geol 63:101–108

Gaboreau S, Cuney M, Quirt D, Beaufort D, Patrier D, Mathieu R (2007) Significance of aluminum phosphate-sulphate minerals associated with U unconformity-type deposits: the Athabasca Basin. Can Am Miner 92:267–280

German CR, Elderfield H (1990) Application of the Ce anamoly as a palaeoredoxindicator: the ground rules. Paleocenagraphy 5:823–833

Hey MH (1954) A new review of the chlorite. Mineral Mag 30:277–292

Hoeve J, Quirt D (1987) A stationary redox front as a critical factor in the formation of high grade unconformity-type uranium ores in the Athabasca basin, Saskatchewan, Canada. Bull De Min 110:157–171

Hower J, Eslinger EV, Hower ME, Perry EA (1976) Mechanism of burial metamorphism of argillaceous sediments: Mineralogical and chemical evidence. Geol Soc Am Bull 87:725–737

Iida Y (1993) Alteration and ore-forming processes of unconformity related uranium deposits. Resour Geol Spec Issue 15:299–308

Iman MB, Shaw EHF (1985) The diagenesis of Neogene clastic sediments from the Bengal Basins Bangladesh. J Sediment Petrol 55:665–671

Jackson ML (1969) Soil chemical analysis—advanced course, 2nd edn. Parallel Press, Madison, p 895

Jakson ML (1985) Soil chemical analysis advance course, 2nd edn. Parallel Press, Madison, pp 100–166

Jha SK, Shrivastava JP, Bhairam CL (2012) Clay mineralogical studies on Bijawars of the Sonrai Basin: palaeoenvironmental implications and inferences on the uranium mineralization. Geol Soc India 79:117–134

Keil RG, Monflugon DB, Prahl FG, Hedges JI (1994) Sorptive preservation of labile organic matter in marine sediments. Nature 370:549–552

Khan KF, Dar SA, Khan SA (2012) Rare earth element (REE) Geochemistry of phosphorites of the Sonrai area of Paleoproterozoic Bijawar basin, Uttar Pradesh, India. J Rare Earths 30:507

Kister P, Laverret E, Quirt D, Cuney M, Patrier Mas P, Beaufort D, Bruneton D (2006) Mineralogy and geochemistry of the host-rock alterations associated with the Shea Creek unconformity-type uranium deposits (Saskatchewan, Canada). Part 2. Regional scale spatial distribution of the Athabasca Group sandstone matrix minerals. Clays Clay Min 54:295–313

Kumar S, Singh MP (1978) Pahoehoe toes in the basic volcanic flow of the Bijawar Group Kurrat area, Lalitpur district, Uttar Pradesh. Curr Sci 47(20):773

Kuscu M, Ozsoy R, Ozcelik O, Altunsoy M (2016) Earth and environmental sciences symposium trace and rare earth element geochemistry of the black shales in Triassic Kasimlar Formation, Anamas—Akseki Platform, Western Taurids, Turkey, vol 30, p 507

Laverret E, Mas PP, Beaufort D, Kister P, Quirt D, Bruneton P, Clauer N (2006) Mineralogy and geochemistry of the host-rock alterations associated with the shea creek unconformity-type uranium deposits (Athabasca basin, Saskatchewan, Canada). Part 1 Spatial variation of illite properties. Clays Clay Miner 54(3):275–294

Lewan MD, Maynard JB (1982) Factors controlling the proportanility of vanadium and nickel in the bitumen of organic sedimentary rocks. Geochem Cosmochem Acta 46:2547–2560

Liu Z, Zhao Y, Colin C, Siringan FP, Wu Q (2009) Chemical weathering in Luzon, Philippines from clay mineralogy and major-element geochemistry of river sediments. Appl Geochem 24:2195–2205

Madhavaraju J, Lee YI (2009) Geochemistry of the Dalmiapuram Formation of the Uttatur Group (Early Cretaceous), Cauvery basin, southeastern India: implications on provenance and paleo-redox conditions. Rev Mex Cien Geol 26:380–394

Mahadevan TM (1986) Space-time controls in Precambrian uranium mineralisation in India. J Geol Soc India 27:47–62

Mason B, Moore CB (1982) Principals of geochemistry, 4the edn. Wiley, New York

Masuda A, Kawakami O, Dohmoto Y, Takenaka T (1987) Lanthanide tetrad effects in nature: two mutually opposite types, W and M. Geochem J 21:119–124

McLennan SM (1989) Rare earth elements in sedimentary rocks: influence of provenance and sedimentary processes. Rev Miner 21:170–199

Mclennan SM (2001) Relationships between the trace element composition of sedimentary rocks and upper continental crust. Geochem Geophys Geosyst 2:2000GC000109

Mercadier J, Cuney M, Lach P, Boiron MC, Bonhoure J, Richard A, Leisen M, Kister P (2011) Origin of uranium deposits revealed by their rare earth element Signature. Terra Nova 23:264–269

Meunier A, Velde B (1989) Solid solution in I/S mixed-layer minerals and illite. Am Mineral 74:1106–1112

Meunier A, Velde B (2004) Illite origins, evolution and metamorphism. Springer, Berlin

Middelburg JJ, Van der Weijden CH, Woittiez JRW (1986) Chemical processes affecting the mobility of major, minor and trace elements during weathering of granitic rocks. Chem Geol 68:253–273

Millot G (1970) Geology of clays. Springer, NewYork

Mishra B (1996) Annual report on the exploratory drilling at Sonrai, Lalitpur District, UP, AMD

Morichon E, Allard T, Beaufort D, Quirt D (2010) An EPR study of native radiation- induced paramagnetic defects in sudoite (di-trioctahedral Al-Mg chlorite) from the alteration halo related to unconformity-type uranium deposits. Phys Chem Miner 37(3):145–152

Nadeau PH, Bain DC (1986) Composition of some smectites and diageneticillitic clays and implications for their origin. Clays Clay Miner 34:455–464

Nance WB, Taylor SR (1976) Rare earth element patterns and crustal evolution, I. Australian post-Archean sedimentary rocks. Geochim Cosmochim Acta 40:1539–1551

Nesbitt HW (1979) Mobility and fractionation of rare earth elements during weathering of a granodiorite. Nature (London) 279:206–210

Nesbitt HW, Young GM (1984) Prediction of some weathering trends of plutonic and volcanic rocks based on thermodynamic and kinetic considerations. Geochim Cosmochim Acta 48:1523–1534

Nutt CJ (1989) Chloritization and associated alteration at the Jabiluka Unconformity-Type Uranium deposit, Northern Territory, Australia. Can Mineral 27:41–58

Pacquet A, Weber F (1993) Petrographie et mineralogie des halos d'alteration autour dugisement de Cigare Lake et leurs relations avec les mineralisations. Can J Earth Sci 30:674–688

Percival JB, Kodama H (1989) Sudoite from Cigar Lake, Saskatchewan. Can Mineral 27:633–641

Pohl WL (2011) Economic geology principles and practice, 1st edn. Wiley, New York

Prakash R, Swarup P, Srivastava RN (1975) Geology and mineralization in the southern parts of Bundelkhand in Lalitpur dist., U.P. J Geol Soc India 16:143–156

Rawat TPS, Roy M, Sharma M, Misra P, Parihar PS, Bhairam CL (2010) Potentiality of Proterozoic Bijawar basin and its environs for unconformity related uranium mineralization in Bundelkhand craton, Central India. Explor Res At Miner 20:27–42

Rawat TPS, Roy M, Joshi GB (2018) Hydrothermal fracture controlled Vein type Uranium mineralization in the Paleoproterozoic Bijawar Group of rocks, Sonrai Basin, Lalitpur district, U.P.—fresh findings from subsurface borehole data. J Geol Soc India 91:25–31

Rene M (2008) Anomalous rare earth element, yttrium and zirconium mobility associated with uranium mineralization. Terra Nova 20:52–58

Rollinson H (1993) Using geochemical data: evaluation, presentation, interpretation. Taylor & Francis, London, pp 102–212

Ross CS, Hendricks SB (1945) Minerals of the montmorillonite group. US Geol Surv Prof Pap 205:23–47

Roy M, Bagchi AK, Babu EVSSK, Mishra B, Krishnamurithy P (2004) Petromineragraphy and mineral chemistry of bituminous shale-hosted uranium mineralization at Sonrai, Lalitpur district, Uttar Pradesh. J Geol Soc India 63:291–298

Roy M, Rawat TPS, Bhairam CL, Parihar PS (2014) Diverse mode of phosphatic rocks in the environs of proterozoic bijawar and sonrai basins and its relevance to uranium mineralisation—a case study from Central India Ross CS, Hendricks SB (1945). Minerals of the montmorillonite group. US Geol Surv Prof Pap 205:23–47

Ruzicka V (1993) Unconformity-type uranium deposits. In: Kirkham RV, Sinclair WD, Thrope RI, Duke JM (eds) Mineral deposits modeling: Geological Association of Canada, special papar, vol 40. Springer, New York, pp 125–149

Sharma KK, Rahman A (2000) The early Archaean Palaeoproterozoic crustal growth of the Bundelkhand craton, northern Indian shield. In: Dev M (ed) crustal evolution and metallogeny in the northwestern Indian Shield. Narosa Publishing House, New Delhi, pp 51–72

Shau YH, Peacor DR (1989) Phyllosilicates in hydrothermally altered basalts from DSDP Hole 504B, Leg 83—a TEM/AEM study (abstract). Geological Society of America, Abstracts with Program, 21

Singer A (1984) The paleoclimatic interpretation of clay in sediments a-Review. Ear Sci Rev 21:251–293

Srivastava RN (1989) Bijawar phospharites at Sonrai-Geology, sedimentation, exploration strategy and origin. Mem Geol Soc India 13:47–59

Srodon J, Drits VA, Mccarty DK, Hsieh JCC, Eberl DD (2001) Quantitative X-ray diffraction analysis of clay-bearing rocks from random preparations. Clays Clay Miner 49(6):514–528

Stevko M, Uher P, Ondrejka M, Ozdin D, Bacik P (2014) Quartz–apatite–REE phosphates–uraninite vein mineralization near Cucma (eastern Slovakia): a product of early Alpine hydrothermal activity in the Gemeric Superunit, Western Carpathians. J Geosci 59:209–222

Takahashi Y, Yoshida H, Sato N, Hana K, Yusa Y, Shimizu H (2002) W- and M-type tetrad effects in REE patterns for water-rock systems in the Tono uranium deposit, Central Japan. Chem Geol 184:311–335

Tan KH (2005) Soil sampling, preparation, and analysis, 2nd edn, Emeritus Professor, University of Georgia, Greensboro, USA, pp 1–623

Taylor SR, McLennan SM (1985) The continental crust: its composition and evolution. Wiley, New York

Thiry M (2000) Paleoclimatic interpretation of clay minerals in marine deposits: an outlook from the continental origin. Ear Sci Rev 49:201–221

Wanty RB, Goldhaber M (1992) Thermodynamics and kinetics of reactions involving vanadium in natural systems: accumulation of vanadium in sedimentary rocks. Geochim Cosmochim Acta 56(4):1471–1483

Weaver CE (1989) Clays, muds and shales. Dev Sedimentol 44:819

Wei G, Liu Y, Xian-hua Li, Shao L, Fang D (2004) Major and trace element variations of the sediments at ODP Site 1144, South China Sea, during the last 230 ka and their paleoclimate implications. Palaeogeog Palaeoclim Palaeoeco 212:331–342

Wilkinson JJ, Chang Z, Cooke DR, Baker MJ, Wilkinson CC, Inglis S, Chen H, Gemmell JB (2015) The chlorite proximitor: a new tool for detecting porphyry ore deposits. J Geochem Explor 152:10–26

Wilson MJ (1987) X-ray powder diffraction methods handbook of determinative methods in clay mineralogy. Blackie, Glasgow, pp 26–98

Wood SA (1996) The Role of Humic substances in the transport and fixation of metals of economic interest (Au, Pt, U, V). Ore Geol Rev 11(1–3):1–31

Wronkiewicz DJ, Condie KC (1989) Geochemistry and provenance of sediments from the pongola supergroup, South Africa: evidence for 3.0 Ga old continental craton. Geochim Cosmochim Acta 53:1537–1549

Yang YL, Aplin AC (1997) A method for the disaggregation of mudstones. Sedimentology 44:559–562

Zhaoliang S, Congqiang L, Guilin H, Zhongliang W, Zhaozhou Z, Cheng Y (2006) Enrichment and release of rare earth elements during weathering of sedimentary rocks in Wujiang catchments Southwest China. J Rare Earth 24:491–496